NATIONAL ADVISORY COMMITTEE FOR AERONAUTICS

TECHNICAL NOTE 3966

THEORETICAL INVESTIGATION OF THE EFFECTS OF CONFIGURATION CHANGES ON THE CENTER-OF-PRESSURE SHIFT OF A BODY-WING-TAIL COMBINATION DUE TO ANGLE OF ATTACK AND MACH NUMBER AT TRANSONIC AND SUPERSONIC SPEEDS

By J. Richard Spahr

Ames Aeronautical Laboratory
Moffett Field, Calif.

Washington

May 1957

iP

NATIONAL ADVISORY COMMITTEE FOR AERONAUTICS

TECHNICAL NOTE 3966

THEORETICAL INVESTIGATION OF THE EFFECTS OF CONFIGURATION CHANGES ON THE CENTER-OF-PRESSURE SHIFT OF A BODY-WING-TAIL COMBINATION DUE TO ANGLE OF ATTACK AND MACH NUMBER AT TRANSONIC AND SUPERSONIC SPEEDS[1]

By J. Richard Spahr

SUMMARY

A theoretical investigation was made to study the effects of systematic changes in configuration of a representative airframe on the center-of-pressure travel due to changes in angle of attack and in Mach number. This airframe was an unbanked canard missile configuration having low-aspect-ratio coplanar wing and tail surfaces of triangular plan form. Each of the following geometric parameters, which define the relative size, plan form, and position on the body of the wing and tail surfaces, was varied while the remaining parameters were held constant: (1) ratio of wing semispan to tail semispan, (2) ratio of body radius to wing semispan, (3) ratio of tail length to body length, (4) wing aspect ratio, (5) tail aspect ratio, (6) wing taper ratio, (7) tail taper ratio, (8) wing sweep, (9) tail sweep, (10) ratio of tail height (vertical distance of tail above body axis) to body radius, and (11) tail roll angle. An angle-of-attack range of 0° to 10° and a Mach number range of 0.6 to 2.0 were covered in the investigation, and the theoretical method described and verified by experiment in NACA Rep. 1307 was used as a basis for the calculations.

The center-of-pressure shift due to an increase in angle of attack was influenced primarily by a single geometric parameter - the ratio of wing semispan to tail semispan. This shift was rearward, and was greatest at a wing-tail semispan ratio near unity. The center-of-pressure shift due to a change in Mach number, however, was influenced significantly by most of the geometric parameters defining the relative size and plan form of the wing and tail surfaces. The total center-of-pressure travel due to the combined effects of angle of attack and Mach number in either the transonic or the supersonic range can be controlled by variations in the configuration geometry. However, only a small degree of control can be exerted over the total center-of-pressure travel through the transonic and supersonic Mach number range by variations in geometry because most of the important configuration changes cause the center of pressure in the transonic range to

[1]Supersedes recently declassified NACA RM A55F02 by J. Richard Spahr, 1955.

move in the opposite direction from that for the supersonic range. Significant reductions in the drag due to longitudinal trim can be realized by the proper choice of configuration to give a minimum center-of-pressure travel.

INTRODUCTION

The longitudinal variations in the center-of-pressure location due to changes in attitude and in Mach number can cause large changes in the maneuverability, performance, and guidance characteristics of a high-speed aircraft (e.g., the drag due to longitudinal trim of the airframe and the frequency response of the automatic control system). For a configuration to have low drag due to trim and adequate frequency response, the center-of-pressure travel due to changes in angle of attack and Mach number must be small.

Only limited experimental or theoretical information is currently available on the effects of configuration changes on the center-of-pressure travel. The results reported in reference 1 indicate that the ratio of wing span to tail span has a large influence on the center-of-pressure shift due to angle of attack, and data from numerous sources, similar to those which have been collected in reference 2, indicate that the wing and tail plan forms have only a small effect on this center-of-pressure shift. The experimental and theoretical results of reference 2 have shown that for a wide variety of missile and airplane configurations, the angle-of-attack effects on the center-of-pressure position might be as large as the Mach number effects.

Because of the lack of adequate information concerning the effects of configuration geometry on center-of-pressure shift due to changes in angle of attack and in Mach number and because of the importance of such effects, the present theoretical investigation was undertaken. This investigation consisted of a systematic study of the separate effects on the center-of-pressure shift of those geometric parameters which define the relative size, plan form, and position on the body of the wing and tail surfaces. The objectives of this theoretical study were:

(1) To investigate the degree of control which the designer can exert over the center-of-pressure travel due to changes in angle of attack and Mach number by varying the configuration geometry.

(2) To determine the configuration variations which lead to zero center-of-pressure shift due to angle of attack or Mach number and those which lead to a minimum shift due to the combined effects of angle of attack and Mach number.

(3) To evolve general design principles for selecting a body-wing-tail combination having a desired center-of-pressure variation with angle of attack and Mach number.

The theoretical method used to compute the center-of-pressure positions is that of reference 2 which provides a reliable prediction of the experimental center-of-pressure position for a wide variety of body-wing-tail combinations at angles of attack up to about 10° and at subsonic, transonic, and supersonic Mach numbers.

NOTATION

Primary Symbols

A	aspect ratio of exposed panels joined together
C_D	drag coefficient due to lift of body-wing-tail combination in untrimmed condition ($\delta = 0$), $\frac{\text{drag}}{qS}$
C_{D_t}	drag coefficient due to lift of body-wing-tail combination in trimmed condition ($C_m = 0$), $\frac{\text{drag}}{qS}$
ΔC_D	drag coefficient due to trim, $C_{D_t} - C_D$
C_L	lift coefficient of body-wing-tail combination, $\frac{\text{lift}}{qS}$
C_{L_α}	$\left(\frac{dC_L}{d\alpha}\right)_{\alpha=0 \text{ and } \delta=0}$
C_{L_δ}	$\left(\frac{dC_L}{d\delta}\right)_{\delta=0 \text{ and } \alpha=0}$
C_m	pitching-moment coefficient of body-wing-tail combination about center of gravity, $\frac{\text{pitching moment}}{qSl}$
c	local chord
c_r	root chord (at juncture of lifting surface and body), figure 1(a)
c_t	tip chord, figure 1(a)
h	tail height above body axis
l	length of body, figure 1(a)

$\bar{l}$	distance from most forward point of body to center of pressure of body-wing-tail combination, figure 1(a)
l_T	tail length, distance between the centroids of area of the exposed wing and tail surfaces, figure 1(a)
M	Mach number
q	dynamic pressure
r	local body radius, figure 1(a)
S	reference area
s	semispan of lifting surface, distance from body axis to tip of surface, figure 1(a)
s_o	static margin, longitudinal distance of the center of pressure of the complete configuration from the center of gravity (positive when center of pressure is behind center of gravity)
$x_{\Lambda=0}$	distance from leading edge along the local chord to the chord line which is unswept
$(x/c)_{\Lambda=0}$	fractional-chord line that is unswept
α	angle of attack
δ	control deflection
λ	taper ratio of lifting surface, $\frac{c_t}{c_r}$
φ	angle of roll about body axis (positive counterclockwise when viewed streamwise)

Subscripts

BW	body-wing combination (less nose)
BT	body-tail combination (less nose)
N	nose portion of body
T	tail
W	wing

ANALYSIS

The longitudinal center-of-pressure locations of several families of body-wing-tail combinations were calculated for angles of attack from 0° to 10° and for Mach numbers from 0.6 to 2.0. These combinations were derived from systematic variations in the geometry of an example configuration. The configurations and theoretical method are described in the following paragraphs.

Basic Configuration

The body-wing-tail combination selected as the basic configuration is shown in figure 1(b) and, except for the afterbody shape, is the same as that tested in reference 3. The basic configuration was selected on the basis of the following considerations: (1) It has a relatively small experimental variation in center of pressure over the Mach number range (see fig. 2); (2) this variation is satisfactorily predicted by the theoretical method of reference 2 (see fig. 2); and (3) the configuration is representative of actual canard missiles.

Configuration Changes

Changes from the basic configuration were made by systematic variations in eleven geometric parameters which define the relative size, position, and plan form of the wing and tail surfaces. The body shape, the longitudinal location of the exposed-wing centroid of area, and the wing roll angle were maintained constant. Each geometric parameter was varied over a wide range while the remaining parameters were held fixed at the values for the basic configuration. These parameters, their range of variation, and their values for the basic configuration are given in the following table:

Parameter	Range of values	Value for basic configuration
s_W/s_T	0 to 2.1	0.484
$(r/s)_W$	0.2 to 1.0	.467
l_T/l	0.2 to 0.68	.456
A_W	0.6 to 3.5	2.31
A_T	0.6 to 3.5	2.31
λ_W	0 to 1	0
λ_T	0 to 1	0
$(x/c)_{\Lambda_W=0}$	0 to 1	1
$(x/c)_{\Lambda_T=0}$	0 to 1	1
$(h/r)_T$	0 to 4	0
φ_T	0° and 45°	0°

Examples of each of these variations in the configuration geometry are illustrated in figure 3 in which the configurations corresponding to altered values of each parameter are given by the dashed lines and the basic configuration by the solid lines.

It should be noted that although the eleven factors varied in this investigation completely define the relative size, position, and plan form of the wing and tail surfaces, the selection of these parameters was arbitrary, and thus alternate parameters could have been used in place of many of those selected. For example, the ratio of the wing area to tail area could have been selected in place of the corresponding span ratio, or the ratio of the body radius to the tail semispan in place of the ratio of the body radius to the wing semispan. It is apparent that these alternate geometric characteristics vary simultaneously with those parameters selected for the present investigation.

Theoretical Method

The center-of-pressure locations for the various configurations at all of the angles of attack and Mach numbers investigated were calculated by the method of reference 2 which is based primarily on linear theory. For the coplanar configuration (wing and tail surfaces in line, $(h/r)_T$ and φ_T are zero), this method was applied directly as presented in reference 2. For the multiplanar configurations (tail surfaces elevated, $(h/r)_T > 0$, or interdigitated, $\varphi_T = 45^\circ$, with respect to the wing surfaces), certain modifications were required to apply the method. For configurations having values of the tail-height parameter $(h/r)_T$ greater than 1, it was assumed that no body-tail interference was present. For values near 1, of course, this assumption would not be expected to be valid, and thus the absolute center-of-pressure positions for these cases may be in error. However, the variations of center of pressure with angle of attack are qualitatively correct. For configurations having the cruciform tail rolled ($\varphi_T = 45^\circ$), the wing-tail interference charts of reference 2 were used directly to calculate the normal force on each of the four tail panels. The center-of-pressure position was then determined from the component of these forces normal to the plane of the wing. The center-of-pressure location and lift-curve slope of a body-wing or body-tail combination predicted by this method are independent of angle of attack. Thus, any change in the center-of-pressure location of a body-wing-tail combination with angle of attack is attributable entirely to wing-tail interference effects.

Because of the assumptions and limitations inherent in the theoretical method, certain approximations and restrictions were imposed on the investigation. The use of linear theory precluded the consideration of large angles of attack, high supersonic Mach numbers, or nonlinear effects in the transonic range. The use of slender-body theory required in the calculation of the body-wing and body-tail interference factors excluded

configurations having wing or tail plan forms with sweptforward leading edges, sweptback trailing edges, or inverse taper ($\lambda > 1$). In addition, the investigation was restricted to rigid airframes having no wing or tail incidence.

RESULTS AND DISCUSSION

The results of this investigation show that except for configurations having nearly equal wing and tail spans, the variations of center-of-pressure location with angle of attack are essentially independent of the variations with Mach number, as indicated by the typical curves of figure 2. This result has previously been shown in reference 2. Thus, the effects of angle of attack and of Mach number are discussed separately in the following paragraphs. These results, which show the influence of several geometric parameters varied one at a time, should be applied only qualitatively to the simultaneous variation of two or more parameters as the effects are not necessarily additive.

Center-of-Pressure Shift Due to Angle of Attack

The results of the calculations show that the longitudinal variations in the center-of-pressure position with angle of attack for all of the configurations having coplanar wing and tail surfaces ($(h/r)_T$ and φ_T are zero) were qualitatively similar (monotonic variations) to that for the basic configuration (fig. 2). Thus, the center-of-pressure shift due to a fixed increment in the angle of attack from 0° is a significant parameter for comparing the relative importance of the geometric variables. The variations of this parameter for an angle-of-attack increase of 8° $((\bar{l}/l)_{\alpha=8^\circ} - (\bar{l}/l)_{\alpha=0^\circ})$ are presented in figure 4 for several Mach numbers as a function of the nine geometric parameters defining the configurations of figures 3(a) to 3(f) (coplanar wing and tail, $(h/r)_T$ and φ_T are zero).

The results of figure 4 show that in all cases the center-of-pressure shift due to an increase in angle of attack is rearward (in the direction of increasing stability). This result follows directly from the fact that this shift is caused entirely by wing-tail interference effects. At zero angle of attack these effects are maximum and thus the center of pressure is at its most forward position. An increase in the angle of attack from zero causes the center of pressure to move rearward and to approach the position corresponding to no wing-tail interference at large angles of attack. The effects of Mach number on the results of figure 4 are caused entirely by the influence of Mach number on the strength of the wing vortex wake through its effect on the wing lift.

Figure 4(a) shows that a large rearward center-of-pressure shift occurs as the wing-tail semispan ratio is varied over its maximum range. For a value of this ratio somewhat less than 0.2 the wing and tail merge into one surface (see fig. 3(a)), and thus the center-of-pressure shift is zero because of the absence of any wing-tail interference. As the span ratio increases (tail span decreases), the center-of-pressure shift rises rapidly to a maximum at a span ratio near 1. This maximum value corresponds to the condition for which the trailing vortex from each wing panel passes over the tail surfaces at the lateral position for maximum wing-tail interference (download on tail). A further increase in the wing-tail span ratio (decrease in tail span) results in a rapid reduction in the center-of-pressure shift to zero at a span ratio of 2.14 since, for this configuration, the tail vanishes at this value. Figures 4(b) to 4(i) show that the effects of the remaining geometric variables on the center-of-pressure shift due to angle of attack are relatively small. The predominance of the wing-tail span ratio over the other geometric variables is caused by the high sensitivity of the wing-tail interference to the lateral position of the wing trailing vortices relative to the tail span as contrasted to the small influence on wing-tail interference of wing or tail plan-form changes. Thus, it is apparent that in order to exert the greatest control over the variation in center of pressure with angle of attack of an inline configuration, only the wing-tail span ratio need be considered, and that in order to minimize this variation, configurations having nearly equal wing and tail spans should be avoided. These theoretical predictions are in basic agreement with the results of reference 2 which indicated that the wing-tail span ratio has a large effect on the center-of-pressure travel due to angle of attack, but that the effect of the wing and tail plan form is small.

Although the center-of-pressure shift of the basic configuration due to angle of attack (fig. 2) is not considered excessive, it is noted that this shift can be reduced to nearly zero by means of an increase in the tail taper ratio from 0 to 1 (fig. 4(g)). No other geometric variable has this effect without reducing the wing or tail area to nearly zero. An increase in the tail taper ratio causes an outboard shift in the center of pressure of the tail load, and thus has an effect on wing-tail interference which is similar to that caused by an increase in the tail span (decrease in s_W/s_T). Therefore, the wing-tail interference and thus the center-of-pressure shift due to angle of attack are reduced. For configurations having wing-tail span ratios greater than 1, an increase in the taper ratio of the tail would be expected to have the opposite effect since a decrease in the wing-tail span ratio s_W/s_T in this range causes an increase in the center-of-pressure shift (see fig. 4(a)).

The results of the calculations for those configurations having noncoplanar wing and tail surfaces (fig. 3(g) and (h)) are presented in figure 5 for one Mach number. The results for other Mach numbers are qualitatively similar. It is noted that in contrast to the corresponding results for the coplanar configurations just discussed, the center of

pressure moves forward as the angle of attack is increased from zero, and this movement is not monotonic but reverses its trend at some angle of attack. This result is again a wing-tail interference effect. Whenever the tail surfaces are moved out of the plane of the wing, either by translation (fig. 3(g)) or by rotation (fig. 3(h)), the angle of attack for maximum interference is no longer zero. Thus, as the angle of attack of such configurations is increased from zero, the tail plane moves into a region of increased interference accompanied by a forward center-of-pressure travel. This effect reaches a maximum at the angle of attack for which the tail surfaces pass through the wing vortex wake. As the angle is increased further, the reverse trend occurs. It is noted from figure 5 that the variation in center-of-pressure position with angle of attack is considerably more for changes in tail height than for interdigitation of the tail. This difference is caused primarily by the fact that the unrolled displaced tail panels which furnish the entire tail lift pass through the wing vortex wake simultaneously; whereas with the tail rotated 45° with respect to the wing, only two of the four lifting tail surfaces pass through the wake at the same time as the angle of attack is increased from zero. Thus, the effects of wing-tail interference are greater for the displaced tail than for the rotated tail. The relative effects of the other geometric parameters, figures 3(c) to 3(f), on the center-of-pressure shift due to angle of attack for a configuration with a displaced or rotated tail are expected to be similar to those for a configuration having a coplanar wing and tail arrangement.

Center-of-Pressure Shift Due to Mach Number

The results of figure 2 show that a relatively abrupt center-of-pressure shift occurs in the transonic Mach number range. Reference 2 indicates that these effects are typical for body-wing-tail combinations in general, and that the center of pressure can move either forward or rearward within the transonic or supersonic Mach number ranges, depending on the configuration. Thus, in order to study the effects of configuration changes on the center-of-pressure shift due to Mach number, it is necessary to consider the shift in both of these Mach number ranges. Consequently, the variation of the center-of-pressure shift due to an increase in the Mach number from 0.9 to 1.1 and that due to an increase from 1.1 to 2.0 have been computed as functions of the geometric parameters, and the results are presented in figures 6 and 7, respectively.

It is observed from these results that in contrast to the influence of configuration changes on the center-of-pressure shift due to angle of attack, no single geometric parameter dominates the remaining parameters with respect to their influence on the center-of-pressure shift due to a Mach number change. Thus, the analysis of the effects of Mach number on the center-of-pressure position is more complex than that of the effects

of angle of attack. This analysis can be greatly facilitated by a consideration of the following relationship, derived in Appendix A, which defines approximately the center-of-pressure shift due to an arbitrary change in Mach number in terms of the contributions of the configuration components (the body nose has no contribution on the basis of slender-body theory):

$$\Delta\bar{l} = (\bar{l}_{BW} - \bar{l})\frac{S_{BW}}{S}\frac{\Delta C_{L_{BW}}}{C_L} + (\bar{l}_{BT} - \bar{l})\frac{S_{BT}}{S}\frac{\Delta C_{L_{BT}}}{C_L} + \frac{S_{BW}}{S}\frac{C_{L_{BW}}}{C_L}\Delta\bar{l}_{BW} + \frac{S_{BT}}{S}\frac{C_{L_{BT}}}{C_L}\Delta\bar{l}_{BT} \quad (1)$$

The results for the center-of-pressure shift due to Mach number in the transonic and supersonic Mach number ranges are discussed separately in the following paragraphs and interpreted by means of this relationship.

Transonic Mach number range.- Figure 6(a) shows that variations in the geometric parameter s_W/s_T result in a large rate of change with s_W/s_T in the rearward center-of-pressure shift in the transonic Mach number range, especially at small values of s_W/s_T. These changes are related directly to the variation with s_W/s_T in the size of the tail relative to the wing. At small values of s_W/s_T the tail is considerably larger than the wing ($S_{BT} \gg S_{BW}$), and thus the center-of-pressure shift of the body-tail combination (second and fourth terms in eq. (1)) is predominant. Both the lift and center-of-pressure increments of the body-tail combination give a rearward center-of-pressure shift in the transonic range, thus resulting in a large rearward shift in the center of pressure of the combination. The large rate of change in center-of-pressure shift with s_W/s_T at small values of s_W/s_T is caused primarily by the correspondingly large rate of change in the tail area (fig. 3(a)). At values of s_W/s_T greater than 1, the characteristics of the body-wing combination predominate, and the first and third terms of equation (1) become increasingly important. These two terms represent center-of-pressure shifts in opposite directions, the first term causing a forward shift, due to the fact that the quantity $\bar{l}_{BW} - \bar{l}$ is negative, and the third term a rearward shift. Thus, the resultant shift is small in this s_W/s_T region. The deviation in the curve for $\alpha = 0^\circ$ from that for $\alpha = 8^\circ$ at values of s_W/s_T in the vicinity of 1 is caused by the effects of Mach number on the wing-tail interference which is a maximum at these values of s_W/s_T and at $\alpha = 0^\circ$, as previously discussed.

The variation of the center-of-pressure shift in the transonic range with the wing-span parameter $(r/s)_W$ (fig. 6(b)) is the result of changes in the relative influence of the lift increment and of the center-of-pressure shift, of the wing and of the tail surfaces, due to an increase in Mach number in the transonic range. The lift increment of the body-wing combination $\Delta C_{L_{BW}}/C_L$ contributes a forward shift in the center of pressure

of the combination because this increment is positive and the quantity $\bar{l}_{BW} - \bar{l}$ of equation (1) is negative. The lift increment of the body-tail combination $\Delta C_{L_{BT}}/C_L$, on the other hand, contributes a rearward shift in the center of pressure because both this increment and the quantity $\bar{l}_{BT} - \bar{l}$ are positive. The center-of-pressure shift of both the body-wing and body-tail combinations are rearward and thus contribute a rearward shift in the center of pressure of the combination (positive values of the last two terms in eq. (1)).

Figure 6(c) shows that a variation in the tail length has only a small effect on the center-of-pressure shift in the transonic range. This result can be attributed to the fact that the lift increment and center-of-pressure shift of the wing and tail surfaces due to Mach number are independent of their longitudinal position. Thus, the only factors in equation (1) which are influenced by a change in tail length are $\bar{l}_{BW} - \bar{l}$ and $\bar{l}_{BT} - \bar{l}$, and the effects of these changes are essentially compensating.

Figures 6(d) and (e) show that an increase in the wing aspect ratio causes a small reduction in the rearward center-of-pressure shift; whereas an increase in the tail aspect ratio has virtually no effect. These results are caused by the small or compensating effects of aspect ratio on the lift increment and on the center-of-pressure shift of the body-wing or body-tail combination.

Figures 6(f) and (g) show that variations in the wing or tail taper ratio have significant effects on the center-of-pressure shift in the transonic range and that the effect of the wing taper ratio is the opposite to that of the tail. It is noteworthy that an increase in the wing taper ratio to nearly 1 results in the virtual elimination of the transonic center-of-pressure shift. These results are due primarily to the effects of taper ratio on the lift increment of the body-wing or body-tail combinations (first two terms of eq. (1)). Since this lift increment is positive, an increase in the wing taper ratio contributes a forward shift in the center of pressure of the complete combination (because the quantity $\bar{l}_{BW} - \bar{l}$ is negative); whereas an increase in the tail taper ratio contributes a rearward shift (because the quantity $\bar{l}_{BT} - \bar{l}$ is positive).

Figures 6(h) and 6(i) show that variations in the wing or tail sweep exert important influences on the transonic center-of-pressure shift and that, as in the case of variable taper ratio, the effect of the wing sweep is the opposite to that of the tail. It is noted that the rearward transonic center-of-pressure shift of the basic configuration can be reduced to zero or changed to a forward shift by a variation in the wing sweep. The effects of wing or tail sweep on the transonic center-of-pressure shift can be explained in the same way as the effects of taper ratio previously discussed. Thus, the results of figures 6(h) and (i) are caused by the variation in the transonic lift increment of the wing or tail with

sweep, and this increment reaches a maximum at values of $(x/c)_{\Lambda=0}$ near 0.5 (diamond plan form).

Supersonic Mach number range.- Figure 7 shows that all of the geometric parameters except tail length (fig. 7(c)) cause significant changes in the center-of-pressure shift in the supersonic Mach number range. It is noted that in contrast to the results for the transonic range (fig. 6) large forward as well as rearward shifts are caused by these geometric variations. The effects of the geometric parameters on the supersonic center-of-pressure shift can be explained in the same manner as for the transonic shift; that is, by an examination through equation (1) of the effects of these parameters on the lift and center-of-pressure increments of the wing and tail due to a change in Mach number. In general, the differences between the results for the supersonic range and those for the transonic range can be attributed primarily to the fact that an increase in Mach number in the supersonic range causes a reduction in the lift coefficient of the wing or tail; whereas an increase in the transonic range causes a net increase in lift coefficient (see ref. 2). The other factor affecting these differences is the generally smaller center-of-pressure shift of the body-wing and body-tail combinations at supersonic speeds than at transonic speeds. A comparison of the direction of the center-of-pressure shift between these two speed ranges is indicated in the following table in terms of the contribution of each component:

Quantity from equation (1)	Center of pressure shift due to an increase in Mach number	
	Transonic range (M = 0.9 - 1.1)	Supersonic range (M = 1.1 - 2.0)
$\Delta C_{L_{BW}}/C_L$	Forward	Rearward
$\Delta C_{L_{BT}}/C_L$	Rearward	Forward
$\Delta \bar{l}_{BW}$	Rearward	Rearward
$\Delta \bar{l}_{BT}$	Rearward	Rearward

A comparison of figures 6(a) and 7(a) shows that the effect of wing-tail span ratio s_W/s_T on the supersonic center-of-pressure shift at small values of s_W/s_T is considerably less than for the transonic shift. This difference arises from the fact that the center-of-pressure shift of the body-tail combination $\Delta \bar{l}_{BT}$ is small in the supersonic range, whereas a large rearward shift occurs in the transonic range. It is noted that, as in the transonic range, the effect of wing-tail interference on the center-of-pressure shift in the supersonic range is large at values of s_W/s_T in the vicinity of 1, but that this effect causes a rearward shift in the supersonic range (fig. 7(a)) in contrast to a forward shift in the transonic range (fig. 6(a)). This difference is due to the fact that the effect of Mach number on the strength of the wing vortices and hence on

the lift of the tail surfaces in the transonic range is opposite to that for the supersonic range.

An increase in the ratio of the body radius to the wing semispan $(r/s)_W$ is shown in figure 7(b) to cause a change from a rearward to a forward center-of-pressure shift in the supersonic Mach number range. This change is the result primarily of the accompanying reduction in the area of the wing relative to that of the tail (fig. 3(b)). As $(r/s)_W$ is increased, a greater portion of the lift is carried by the tail surfaces because of this area change. Thus, since the lift increment of the body-tail combination (second term in eq. (1)) contributes a forward center-of-pressure shift, the shift of the combination becomes increasingly forward as $(r/s)_W$ is increased.

The negligible effect of tail length on the supersonic center-of-pressure shift (fig. 7(c)) occurs for the same reason as that discussed previously for the transonic range.

Large changes, both forward and rearward, in the center-of-pressure shift in the supersonic range are shown in figures 7(d) and (e) as the result of changes in the wing or tail aspect ratio. These results are caused by the large increase in the lift increment of the wing or tail surfaces due to Mach number when the aspect ratio is increased. An increase in the wing aspect ratio increases the lift decrement of the body-wing combination $((S_{BW}/S)(\Delta C_{L_{BW}}/C_L)$ of eq. (1)) and thus contributes a rearward shift in the center of pressure of the body-wing-tail combination. Similarly, an increase in the tail aspect ratio increases the lift decrement of the body-tail combination and contributes a forward center-of-pressure shift.

The effects of wing or tail taper ratio on the supersonic center-of-pressure shift are shown in figures 7(f) and 7(g) to be large and in the opposite direction to the corresponding effects in the transonic range. This difference is caused by the change in the effect of Mach number on the lift of the wing or tail from an increase at transonic speeds to a decrease at supersonic speeds. Thus, the factors $\Delta C_{L_{BW}}/C_L$ or $\Delta C_{L_{BT}}/C_L$ in equation (1) change from positive to negative between the transonic and supersonic ranges.

The effects of wing or tail sweep on the supersonic center-of-pressure shift (figs. 7(h) and (i)) are also observed to be in the opposite direction to these effects in the transonic range, and the cause of this difference is the same as that just discussed for the taper-ratio effect.

Combined Effects of Angle of Attack and Mach Number

The curves of figures 4, 6, and 7 have shown that the predominant geometric variable influencing the center-of-pressure shift due to angle of attack is different from those having the most effect on the center-of-pressure shift due to Mach number. Thus, it appears possible to control effectively the center-of-pressure shift due to the combined effects of angle of attack and Mach number in either the transonic or supersonic range. For example, the rearward center-of-pressure shift in the transonic Mach number range can be reduced to zero by an increase in the wing taper ratio (fig. 6(f)), without causing a significant change in the center-of-pressure shift due to angle of attack (fig. 4(f)). Likewise, a variation in the geometric parameters defining the size and plan form of the wing and tail surfaces can cause a large forward or rearward center-of-pressure shift in the supersonic range without changing the shift due to angle of attack.

It is noted, however, that the center-of-pressure shift in the transonic range cannot be controlled independently of that in the supersonic range because of the dependence of both of these shifts on many of the same geometric variables. For example, a reduction in the wing taper ratio to decrease the center-of-pressure shift in the transonic range (fig. 6(f)) would result in an increase in the center-of-pressure shift in the supersonic range. Thus, it does not appear possible to reduce to zero the center-of-pressure shift throughout the transonic and supersonic speed range by means of a single geometric variable.

The minimum center-of-pressure shifts due both to angle of attack and to Mach number for each of the parameters investigated are given in the following table along with the corresponding values of these parameters:

Parameter	Value of parameter for basic configuration	Change in angle of attack (fig. 4)		Change in transonic Mach number $\alpha = 8^\circ$ (fig. 6)		Change in supersonic Mach number $\alpha = 8^\circ$ (fig. 7)	
		Center-of-pressure shift	Value of parameter	Center-of-pressure shift	Value of parameter	Center-of-pressure shift	Value of parameter
s_W/s_T	0.484	0	<0.2 and >2.0	0.01	>0.8	0	0.3
$(r/s)_W$	.467	0	1	.017	.7	0	.44
l_T/l	.456	.004	.2	.019	.2	0	.33
A_W	2.31	.01	3	.018	2.5 to 3.5	0	1.7
A_T	2.31	.01	2	.017	3.5	0	2.1
λ_W	0	.01	0	0	1	0	.04
λ_T	0	.001	1	.019	0	0	0
$(x/c)_{\Lambda_W=0}$	1	.01	1	0	0.5 and 0.6	0	0.16 and 0.92
$(x/c)_{\Lambda_T=0}$	1	.01	0 to 1	.009	0	0	0.34 and 1.0

This table provides a convenient means for comparing the effects of the various geometric parameters in minimizing the center-of-pressure shift and shows that a compromise in design is necessary to minimize the center-of-pressure shift through the entire speed range; that is, no single value of any of the parameters results in a zero center-of-pressure shift due to both angle of attack and Mach number in the transonic and supersonic ranges.

The effects of changes in the center-of-pressure location on the trim-drag penalty (increase in drag caused by deflection of the controls to balance the pitching moment) have been estimated in order to determine the importance of these effects. Expressions have been derived in Appendix B for the trim drag of two classes of body-wing-tail combinations, one having the control surfaces forward, which would include the basic configuration of this investigation, and the other having the control surfaces aft. All the quantities in these equations can be predicted by the method of reference 2. It is evident from equations (B9) and (B13) that the trim drag depends only on the lift characteristics of the combination and on the ratio of the static margin to the control moment arm. The trim drag for the basic configuration at a Mach number of 1.1 has been computed from equation (B10) with longitudinal control furnished by all-movable forward surfaces. The static margin s_o/l and the lift derivatives C_{L_α} and C_{L_δ} for this condition were obtained from the experimental results of reference 3, and the remaining quantities were calculated by the method of reference 2. It was found that for an assumed static margin s_o/l of 0.075, the trim-drag factor $\Delta C_D/C_D$ was nearly 0.6. If the rearward center-of-pressure shift in the transonic range $(\bar{l}/l)_{M=1.1} - (\bar{l}/l)_{M=0.9}$ were reduced by only 0.025, the trim-drag factor would be lowered to one-half its value (0.3). Thus, it is apparent that by suitable changes in the configuration, significant reductions in the drag due to longitudinal trim can be realized.

CONCLUSIONS

A theoretical study based on linearized theory was made to investigate the effects of systematic variations in geometry on the center-of-pressure shift of a wing-body-tail combination due to changes in angle of attack and in Mach number in both the transonic and supersonic ranges in order to ascertain the degree of control which a designer can exert over the center-of-pressure travel due to these variables. Each of the geometric parameters which define the relative size, plan form, and position on the body of the wing and tail surfaces were varied one at a time. On the basis of the results of this theoretical analysis, the following conclusions have been drawn:

1. The ratio of wing span to tail span was the predominant geometric variable influencing the rearward center-of-pressure shift due to an

increase in the angle of attack. This shift reached a maximum at a wing-tail span ratio near 1 and approached 0 at span ratios near 0 and 2. Tail height was the only geometric variable which caused a significant forward center-of-pressure shift with angle of attack.

2. The center-of-pressure shift due to an increase in Mach number could be controlled primarily by those geometric parameters which influenced the ratio of the lift carried by the wing to that carried by the tail.

3. The parameters which had the largest influence on the rearward center-of-pressure shift in the transonic Mach number range were the ratio of wing to tail span, the ratio of body radius to wing semispan, and the taper ratio and sweep of the wing or tail. The rearward shift could be reduced to zero by an increase in the wing taper ratio from 0 to 1 or by a reduction in the sweep of the wing midchord line to zero, but very little forward shift could be attained by the parameters investigated.

4. The center-of-pressure shift due to an increase in Mach number in the supersonic range was influenced in either a forward or rearward direction by the ratio of the body radius to wing semispan, wing or tail aspect ratio, or tail sweep. Variations in the wing taper ratio or sweep affected only the rearward center-of-pressure shift; whereas the tail taper ratio affected only the forward shift.

5. The total center-of-pressure travel due to the combined effects of angle of attack and Mach number in either the transonic or supersonic range can be controlled by variations in the configuration geometry because of the independence of the center-of-pressure shift due to angle of attack from that due to Mach number.

6. Only a small degree of control can be exerted over the total center-of-pressure travel through the transonic and supersonic Mach number range by configuration variations because most of the same geometric parameters affect the center-of-pressure shift in both Mach number ranges but in opposite directions.

7. Significant reductions in the drag due to longitudinal trim can be realized by the proper choice of configuration to give a minimum center-of-pressure travel.

Ames Aeronautical Laboratory
National Advisory Committee for Aeronautics
Moffett Field, Calif., June 2, 1955

APPENDIX A

DERIVATION OF EXPRESSION FOR CENTER-OF-PRESSURE SHIFT DUE TO A CHANGE IN MACH NUMBER

The center-of-pressure location and lift of a body-wing-tail combination are defined by the expressions

$$\bar{l} = \bar{l}_N \frac{S_N}{S} \frac{C_{L_N}}{C_L} + \bar{l}_{BW} \frac{S_{BW}}{S} \frac{C_{L_{BW}}}{C_L} + \bar{l}_{BT} \frac{S_{BT}}{S} \frac{C_{L_{BT}}}{C_L} \tag{A1}$$

and

$$C_L = \frac{S_N}{S} C_{L_N} + \frac{S_{BW}}{S} C_{L_{BW}} + \frac{S_{BT}}{S} C_{L_{BT}} \tag{A2}$$

respectively. The change in center-of-pressure location of the combination as a result of a change in the lift or center of pressure of any component is expressed by the differentiation of equation (A1)

$$d\bar{l} = \frac{S_N}{S}\left(\bar{l}_N \frac{dC_{L_N}}{C_L} + \frac{C_{L_N}}{C_L} d\bar{l}_N\right) + \frac{S_{BW}}{S}\left(\bar{l}_{BW} \frac{dC_{L_{BW}}}{C_L} + \frac{C_{L_{BW}}}{C_L} d\bar{l}_{BW}\right) +$$

$$\frac{S_{BT}}{S}\left(\bar{l}_{BT} \frac{dC_{L_{BT}}}{C_L} + \frac{C_{L_{BT}}}{C_L} d\bar{l}_{BT}\right) - \bar{l} \frac{dC_L}{C_L} \tag{A3}$$

A differentiation of equation (A2) gives

$$dC_L = \frac{S_N}{S} dC_{L_N} + \frac{S_{BW}}{S} dC_{L_{BW}} + \frac{S_{BT}}{S} dC_{L_{BT}} \tag{A4}$$

and a combination of equations (A3) and (A4) yields

$$d\bar{l} = (\bar{l}_N - \bar{l})\frac{S_N}{S} \frac{dC_{L_N}}{C_L} + (\bar{l}_{BW} - \bar{l})\frac{S_{BW}}{S} \frac{dC_{L_{BW}}}{C_L} + (\bar{l}_{BT} - \bar{l})\frac{S_{BT}}{S} \frac{dC_{L_{BT}}}{C_L} +$$

$$\frac{S_N}{S} \frac{C_{L_N}}{C_L} d\bar{l}_N + \frac{S_{BW}}{S} \frac{C_{L_{BW}}}{C_L} d\bar{l}_{BW} + \frac{S_{BT}}{S} \frac{C_{L_{BT}}}{C_L} d\bar{l}_{BT} \tag{A5}$$

When the differential quantities of this equation are taken with respect to Mach number, the terms involving the body nose (first and fourth terms)

become zero because of the use of slender-body theory in the present calculations to determine the aerodynamic characteristics of the body nose. This theory gives the well-known result that the lift-curve slope $(C_{L_\alpha})_N$ and the center-of-pressure position of a body are independent of Mach number. Thus, the factors dC_{L_N}/C_L and $d\bar{l}_N$ in equation (A5) are zero when taken with respect to Mach number. Equation (A5) can then be rewritten in the form

$$\Delta\bar{l} = (\bar{l}_{BW} - \bar{l})\frac{S_{BW}}{S}\frac{\Delta C_{L_{BW}}}{C_L} + (\bar{l}_{BT} - \bar{l})\frac{S_{BT}}{S}\frac{\Delta C_{L_{BT}}}{C_L} + \frac{S_{BW}}{S}\frac{C_{L_{BW}}}{C_L}\Delta\bar{l}_{BW} + \frac{S_{BT}}{S}\frac{C_{L_{BT}}}{C_L}\Delta\bar{l}_{BT} \quad \text{(A6)}$$

where the symbol Δ designates the change due to a finite change in Mach number.

APPENDIX B

DERIVATION OF EXPRESSIONS FOR TRIM DRAG

The incremental drag coefficient caused by trimming (reducing the pitching moment about the center of gravity to zero) a body-wing-tail combination at a given lift coefficient is defined as the difference between the drag due to lift in the trimmed condition and that in the untrimmed condition. Expressions for the trim drag for the case of no leading-edge suction are derived in the succeeding paragraphs for the two general classes of longitudinal-control arrangement: (1) wing-forward (canard) control and (2) tail-aft control.

Wing-Forward Control

This class of configuration includes all those in which the longitudinal-control surfaces are forward on the body and are followed by fixed lifting surfaces, the loading on which is influenced by deflection of the controls. The drag due to lift of a configuration in the trimmed ($C_m = 0$) and untrimmed ($\delta = 0$) conditions, respectively, is given by the expressions

$$C_{D_t} = \frac{1}{2} C_{L_{\alpha_N}} \alpha_t^2 + C_{L_{\alpha_{BW}}} \alpha_t^2 + C_{L_{\alpha_{BT}}} (k_1 \alpha_t)^2 + C_{L_{\delta_{BW}}} \delta^2 + C_{L_{\delta_{BT}}} (k_2 \delta)^2 \tag{B1}$$

and

$$C_D = \frac{1}{2} C_{L_{\alpha_N}} \alpha^2 + C_{L_{\alpha_{BW}}} \alpha^2 + C_{L_{\alpha_{BT}}} (k_1 \alpha)^2 \tag{B2}$$

where

α_t angle of attack for trimmed condition ($C_m = 0$)

α angle of attack for untrimmed condition ($\delta = 0$)

k_1 wing-downwash factor due to angle of attack, $\dfrac{C_{L_\alpha} - \left(C_{L_{\alpha_N}} + C_{L_{\alpha_{BW}}}\right)}{C_{L_{\alpha_{BT}}}}$

k_2 wing-downwash factor due to control deflection, $\dfrac{C_{L_\delta} - C_{L_{\delta_{BW}}}}{C_{L_{\delta_{BT}}}}$

Thus, the trim drag is given by the difference between equations (B1) and (B2)

$$\Delta C_D = C_{D_t} - C_D = \left(\frac{1}{2} C_{L_{\alpha_N}} + C_{L_{\alpha_{BW}}} + k_1^2 C_{L_{\alpha_{BT}}}\right)\left[\left(\frac{\alpha_t}{\alpha}\right)^2 - 1\right]\alpha^2 + \left(C_{L_{\delta_{BW}}} + k_2^2 C_{L_{\delta_{BT}}}\right)\delta^2 \tag{B3}$$

The lift and pitching moments about the center of gravity are given by

$$C_{L_t} = C_{L_\alpha}\alpha_t + C_{L_\delta}\delta \tag{B4}$$

$$C_L = C_{L_\alpha}\alpha \tag{B5}$$

$$C_{m_t} = 0 = - s_o C_{L_\alpha}\alpha_t - l_\delta C_{L_\delta}\delta \tag{B6}$$

where

l_δ effective moment arm of the control from the center of gravity, $\frac{l_o C_{L_{\delta_{BW}}} + s_1 k_2 C_{L_{\delta_{BT}}}}{C_{L_\delta}}$ (positive when control is aft of center of gravity)

l_o control moment arm from the center of gravity (positive when control is aft of center of gravity)

Combining equations (B4), (B5), and (B6), and setting $C_L = C_{L_t}$, yields the relations

$$\frac{\alpha_t}{\alpha} = \frac{1}{1 - (s_o/l_\delta)} \tag{B7}$$

and

$$\delta = \frac{- (s_o/l_\delta)}{1 - (s_o/l_\delta)} \frac{C_L}{C_{L_\delta}} \tag{B8}$$

Substituting equations (B7) and (B8) into (B3) gives the result

$$\frac{\Delta C_D}{C_L} = \left\{ \frac{1}{[1 - (s_o/l_\delta)]^2} - 1 \right\} \frac{(1/2)C_{L_{\alpha_N}} + C_{L_{\alpha_{BW}}} + k_1^2 C_{L_{\alpha_{BT}}}}{C_{L_\alpha}} \frac{C_L}{C_{L_\alpha}} +$$

$$\frac{(s_o/l_\delta)^2}{[1 - (s_o/l_\delta)]^2} \frac{C_{L_{\delta_{BW}}} + k_2^2 C_{L_{\delta_{BT}}}}{C_{L_\delta}} \frac{C_L}{C_{L_\delta}} \qquad \text{(B9)}$$

The trim-drag increment expressed as a fraction of the untrimmed drag can be derived similarly which results in the expression

$$\frac{\Delta C_D}{C_D} = \frac{1}{[1 - (s_o/l_\delta)]^2} - 1 +$$

$$\frac{(s_o/l_\delta)^2}{[1 - (s_o/l_\delta)]^2} \frac{C_{L_{\delta_{BW}}} + k_2^2 C_{L_{\delta_{BT}}}}{(1/2)C_{L_{\alpha_N}} + C_{L_{\alpha_{BW}}} + k_1^2 C_{L_{\alpha_{BT}}}} \left(\frac{C_{L_\alpha}}{C_{L_\delta}} \right)^2 \qquad \text{(B10)}$$

It is noteworthy that the trim-drag increment, when expressed in this manner, is independent of the lift coefficient C_L.

Tail-Aft Control

This class of configuration includes all those having no lifting surfaces aft of the control surfaces or those in which the effects of such surfaces can be neglected. For the present purpose, the tail-aft control configuration can be considered a special case of the wing-forward control, namely, one for which the lift on the tail surfaces are not influenced by the downwash due to control deflection. Thus,

$$k_2 = 0$$

$$l_\delta = l_o$$

and

$$C_{L_{\delta_{BW}}} = C_{L_\delta}$$

Therefore, the expressions for the drag increment due to longitudinal trim for a configuration with a tail-aft control corresponding to equations (B9) and (B10) are

$$\frac{\Delta C_D}{C_L} = \left\{\frac{1}{[1 - (s_o/l_o)]^2} - 1\right\} \frac{(1/2)C_{L_{\alpha_N}} + C_{L_{\alpha_{BW}}} + k_1^2 C_{L_{\alpha_{BT}}}}{C_{L_\alpha}} \frac{C_L}{C_{L_\delta}} + \left[\frac{s_o/l_o}{1 - (s_o/l_o)}\right]^2 \frac{C_L}{C_{L_\delta}} \tag{B11}$$

and

$$\frac{\Delta C_D}{C_D} = \frac{1}{[1 - (s_o/l_o)]^2} - 1 + \left[\frac{s_o/l_o}{1 - (s_o/l_o)}\right]^2 \frac{C_{L_\alpha}}{(1/2)C_{L_{\alpha_N}} + C_{L_{\alpha_{BW}}} + k_1^2 C_{L_{\alpha_{BT}}}} \frac{C_{L_\alpha}}{C_{L_\delta}} \tag{B12}$$

For those configurations in which $C_{L_{\alpha_{BT}}} \ll C_{L_{\alpha_{BW}}}$ (or $k_1 \approx 1$) and $C_{L_{\alpha_N}} \ll C_{L_\alpha}$, equations (B11) and (B12) reduce to the simpler forms

$$\frac{\Delta C_D}{C_L} = \left\{\frac{1}{[1 - (s_o/l_o)]^2} - 1\right\} \frac{C_L}{C_{L_\alpha}} + \left[\frac{s_o/l_o}{1 - (s_o/l_o)}\right]^2 \frac{C_L}{C_{L_\delta}} \tag{B13}$$

and

$$\frac{\Delta C_D}{C_D} = \frac{1}{[1 - (s_o/l_o)]^2} - 1 + \left[\frac{s_o/l_o}{1 - (s_o/l_o)}\right]^2 \frac{C_{L_\alpha}}{C_{L_\delta}} \tag{B14}$$

REFERENCES

1. Morikawa, George: Supersonic Wing-Body-Tail Interference. Jour. Aero. Sci., vol. 19, no. 5, May 1952, pp. 333-340.

2. Pitts, William C., Nielsen, Jack N., and Kaattari, George E.: Lift and Center of Pressure of Wing-Body-Tail Combinations at Subsonic, Transonic, and Supersonic Speeds. NACA Rep. 1307, 1957.

3. Niewald, Roy J., and Moul, Martin T.: The Longitudinal Stability, Control Effectiveness, and Control Hinge-Moment Characteristics Obtained from a Flight Investigation of a Canard Missile Configuration at Transonic and Supersonic Speeds. NACA RM L50I27, 1950.

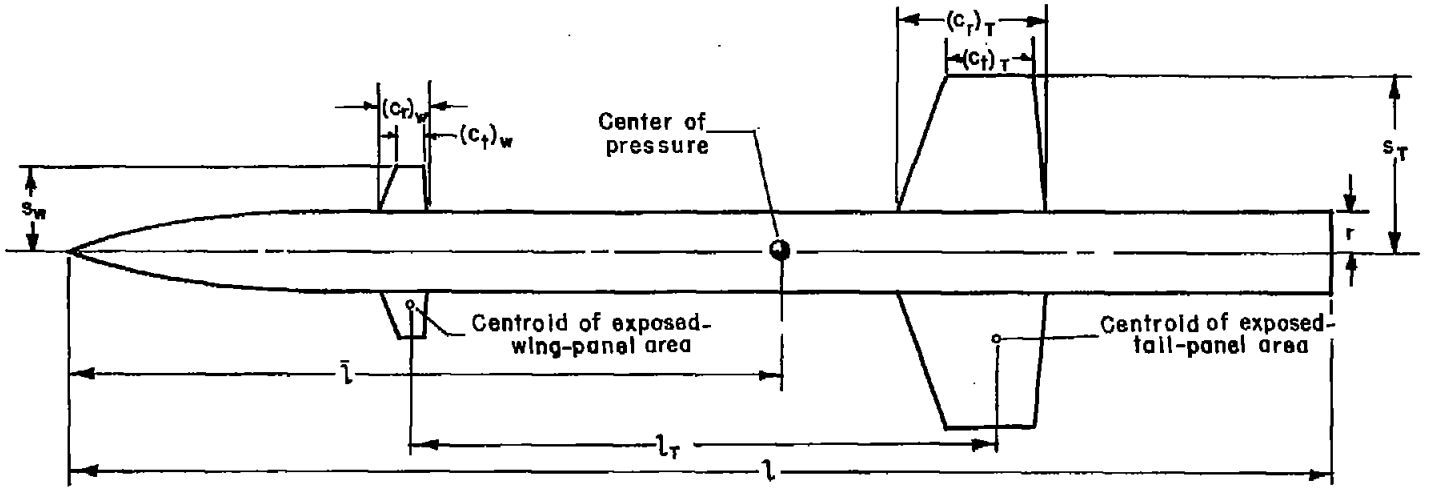

(a) Generalized configuration.

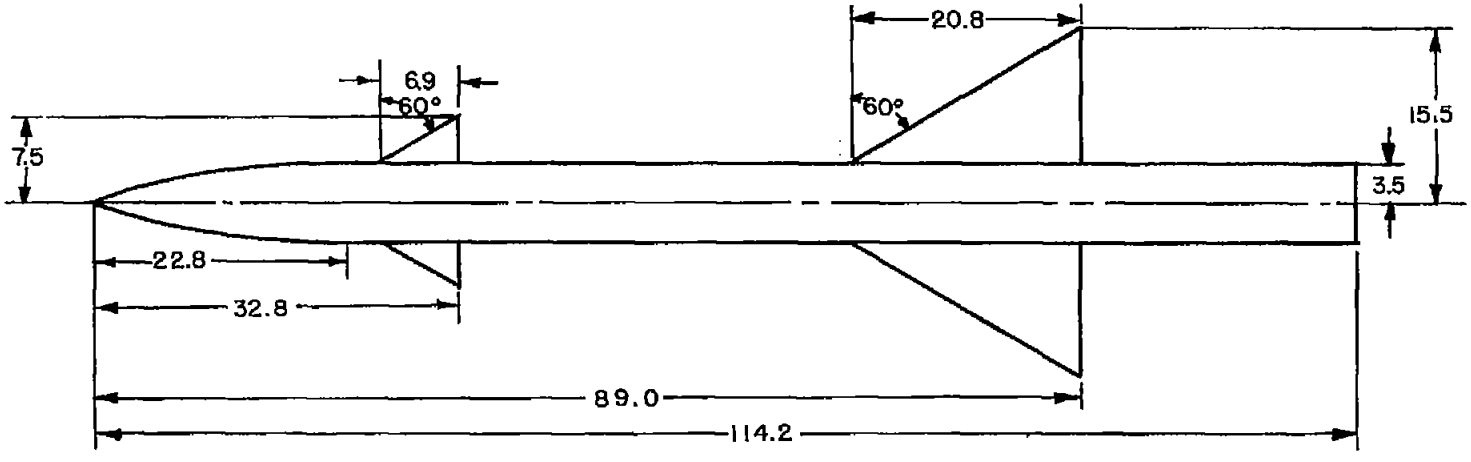

(b) Basic configuration.

Figure 1.- Body-wing-tail combinations. All dimensions in inches.

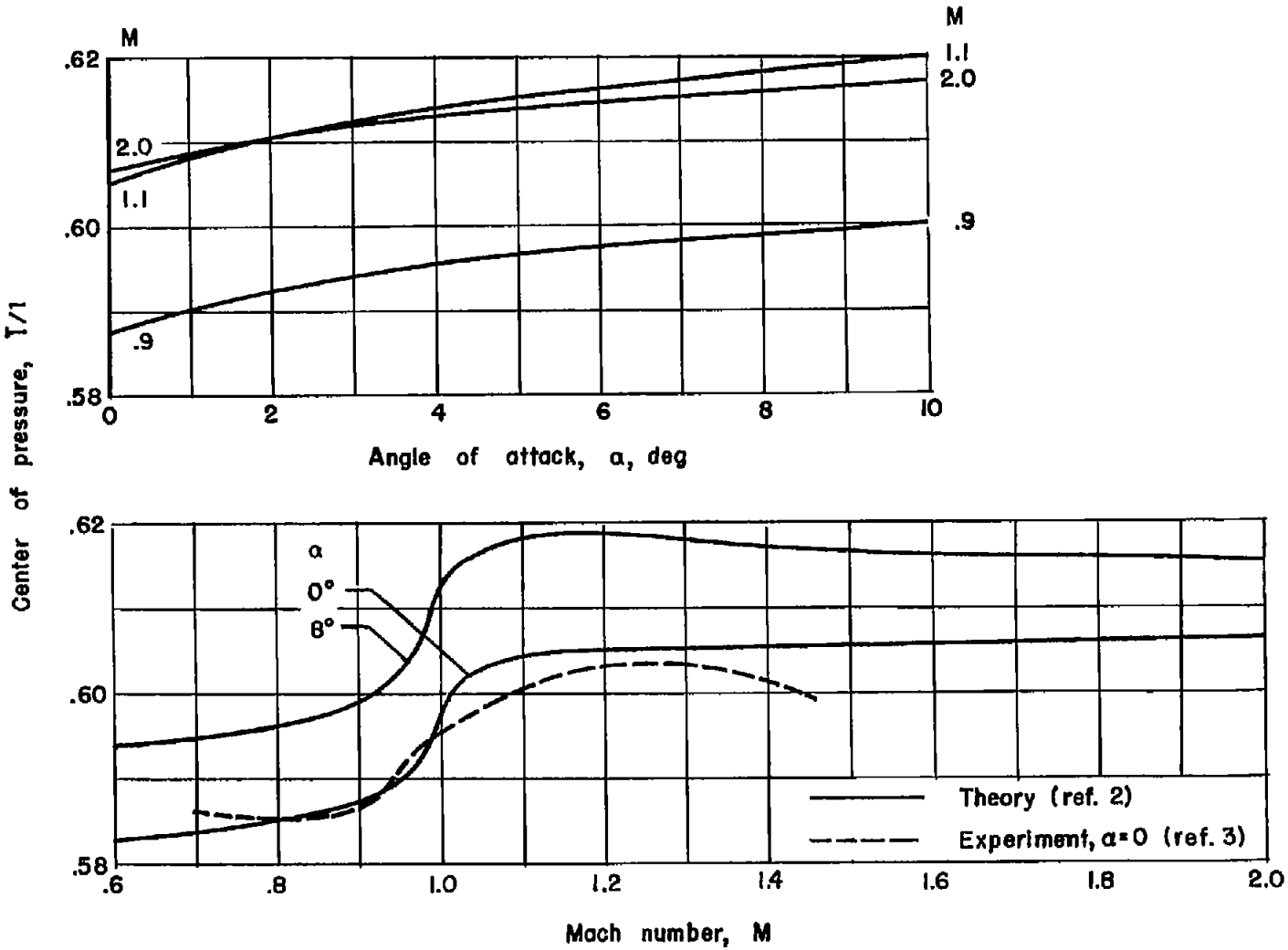

Figure 2.- Effects of angle of attack and Mach number on the center of pressure of the basic configuration.

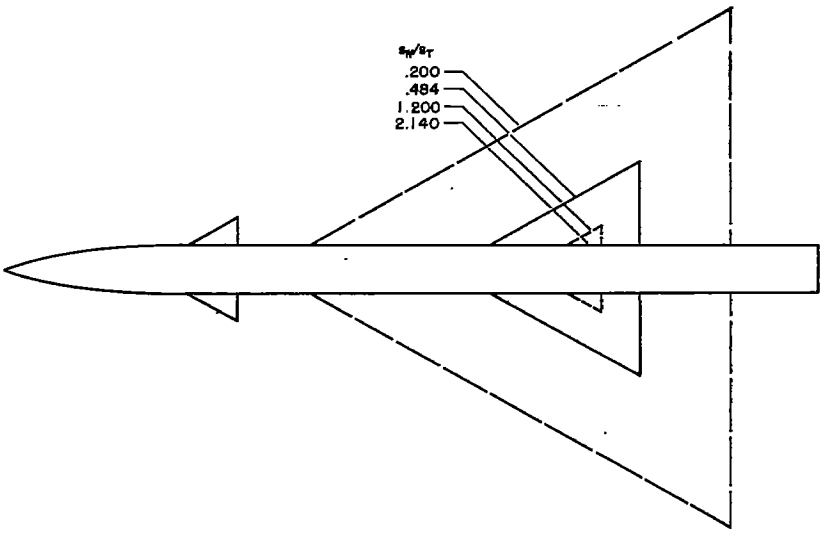

(a) Variable wing-semispan to tail-semispan ratio, s_W/s_T.

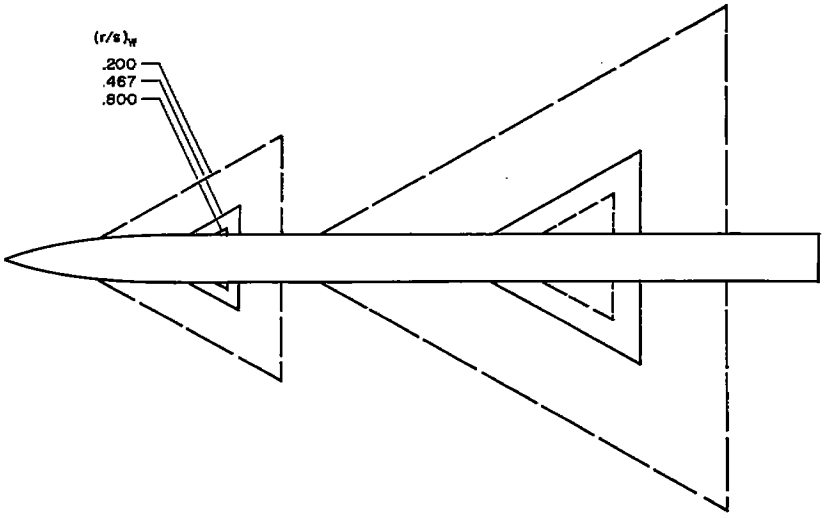

(b) Variable body-radius to wing-semispan ratio, $(r/s)_W$.

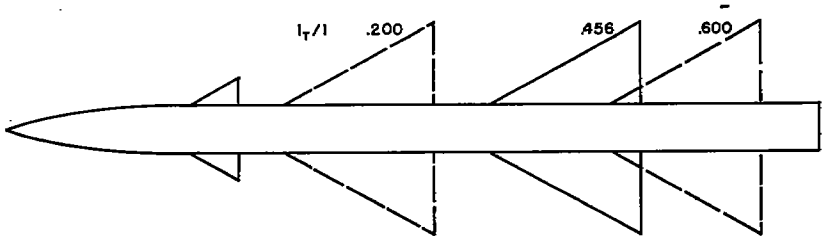

(c) Variable tail length, l_T/l.

Figure 3.- Effects of geometric variables on configuration.

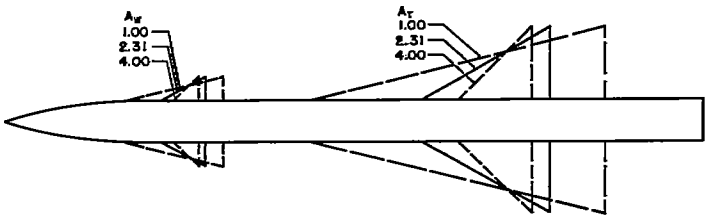

(d) Variable wing and tail aspect ratio, A_W and A_T.

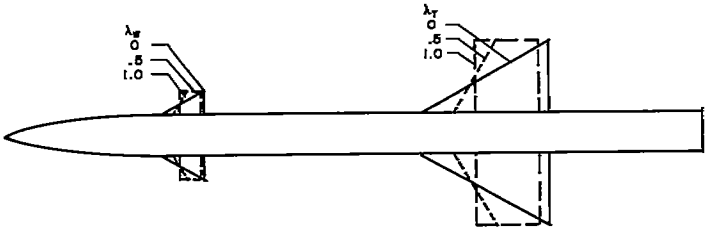

(e) Variable wing and tail taper ratio, λ_W and λ_T.

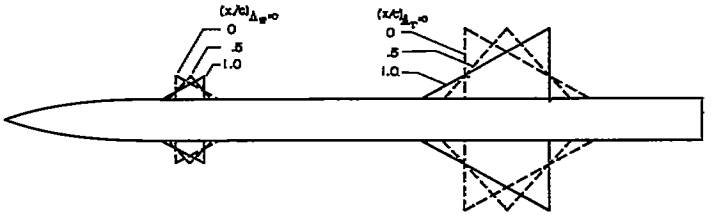

(f) Variable wing and tail sweep, $(x/c)_{\Lambda_W=0}$ and $(x/c)_{\Lambda_T=0}$.

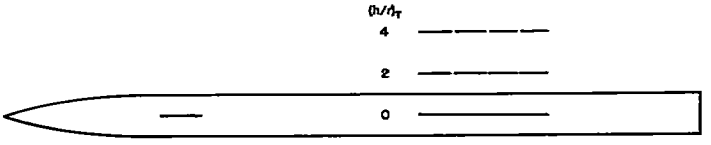

(g) Variable tail height, $(h/r)_T$.

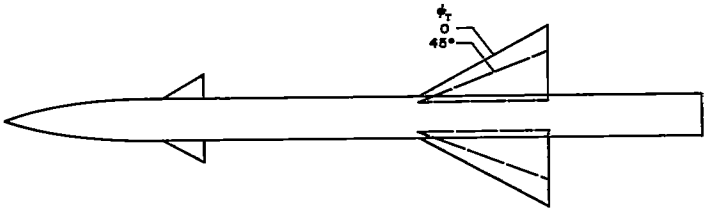

(h) Variable tail roll angle, Φ_T.

Figure 3.- Concluded.

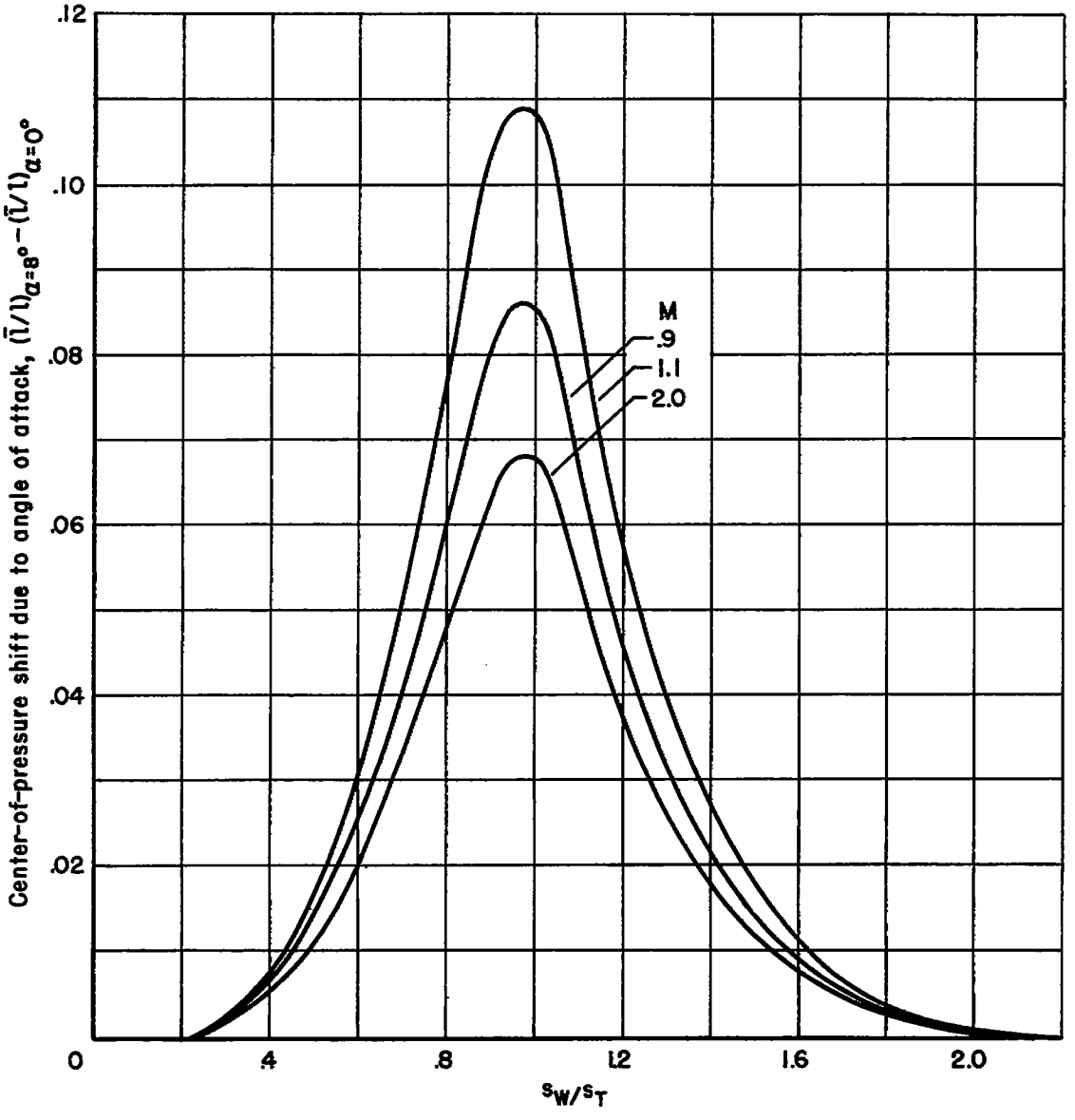

(a) Effect of wing-semispan to tail-semispan ratio.

Figure 4.- Effect of geometric parameters on the center-of-pressure shift due to angle of attack.

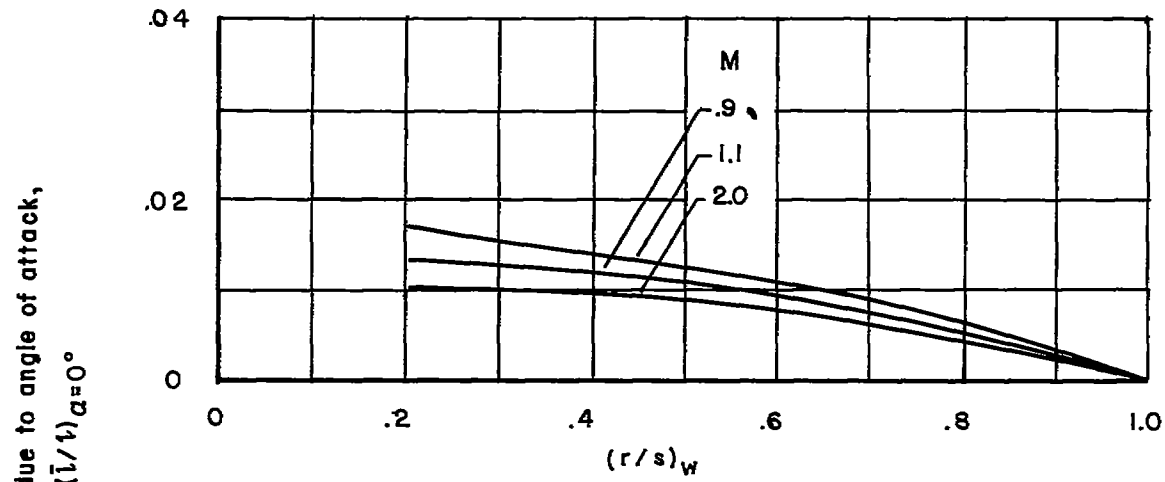

(b) Effect of body-radius to wing-semispan ratio.

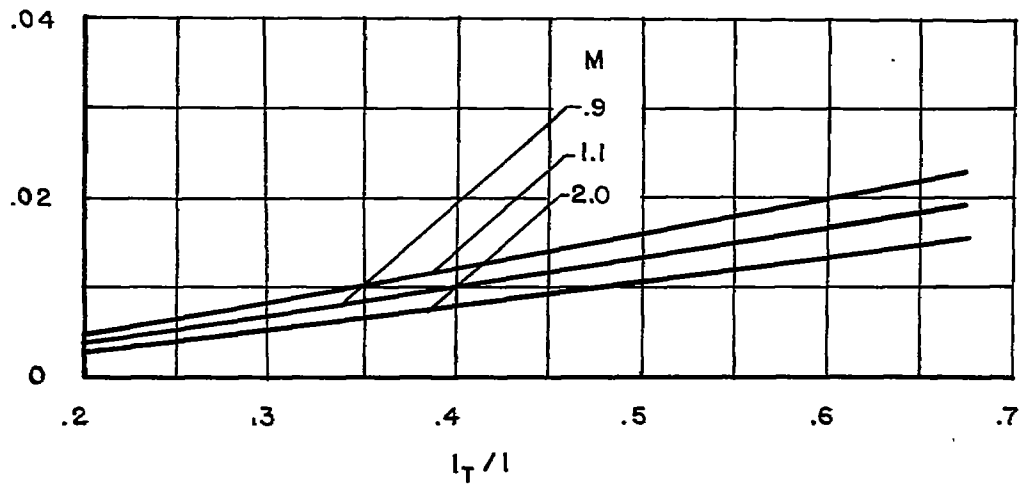

(c) Effect of tail-length to body-length ratio.

Figure 4.- Continued.

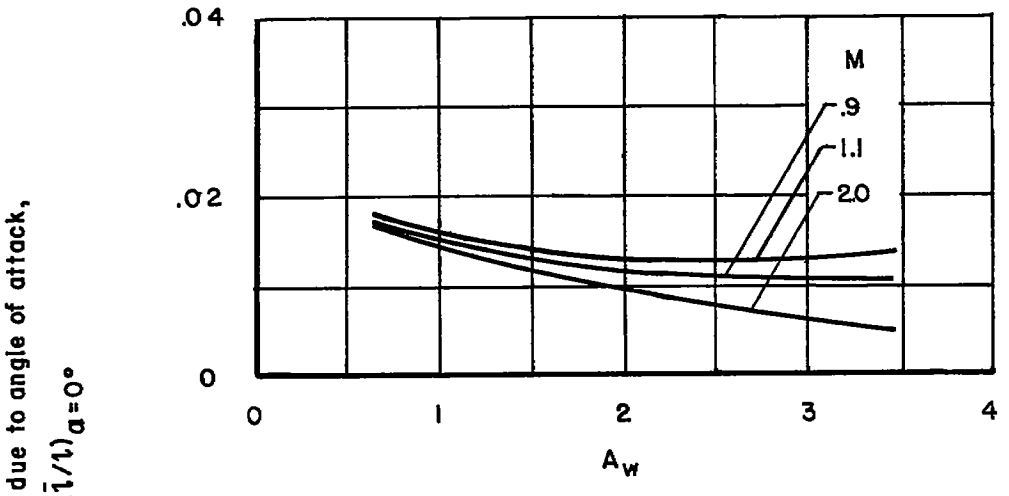

(d) Effect of wing aspect ratio.

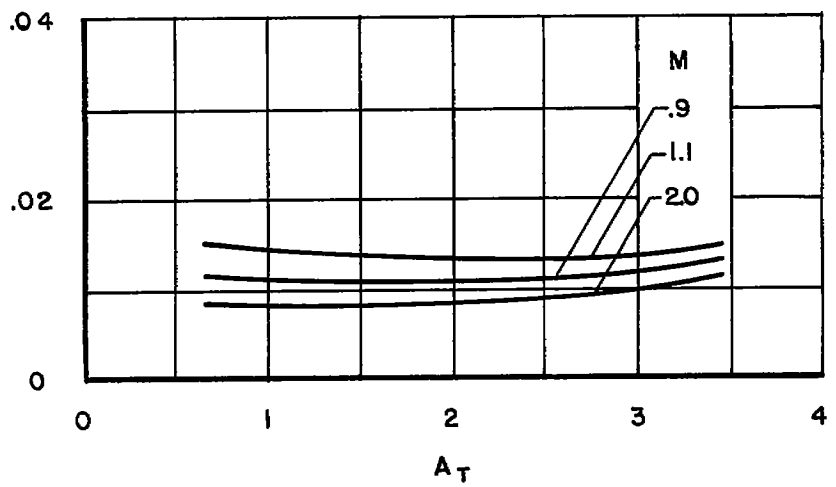

(e) Effect of tail aspect ratio.

Figure 4.- Continued.

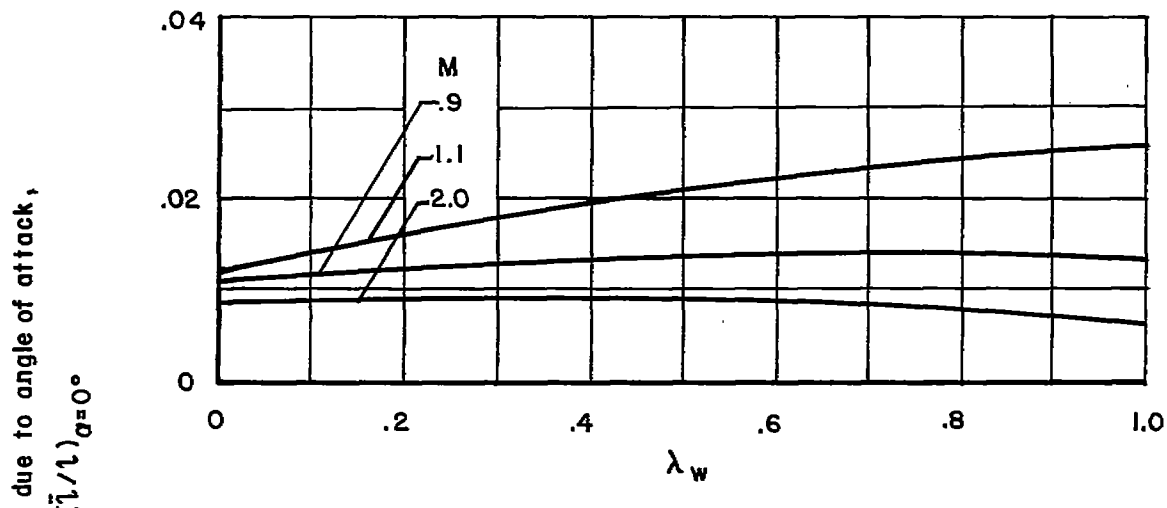

(f) Effect of wing taper ratio.

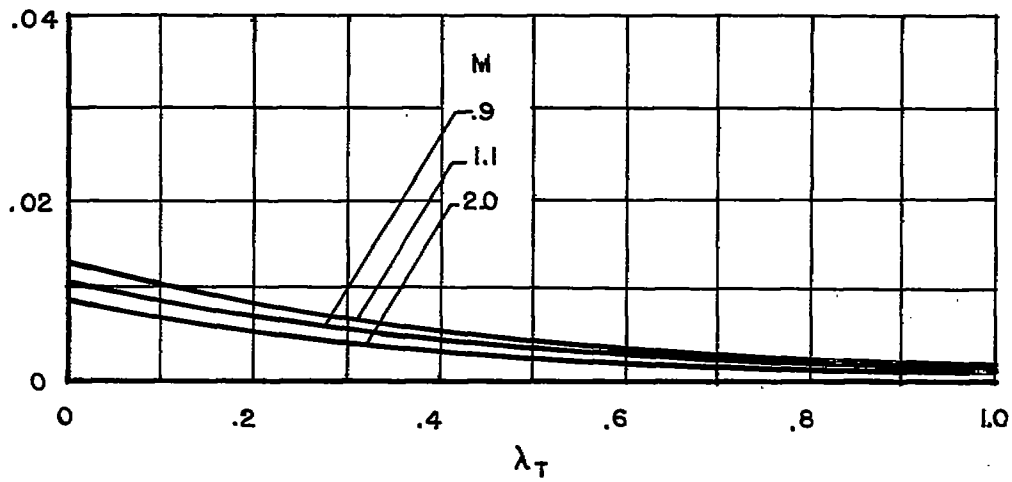

(g) Effect of tail taper ratio.

Figure 4.- Continued.

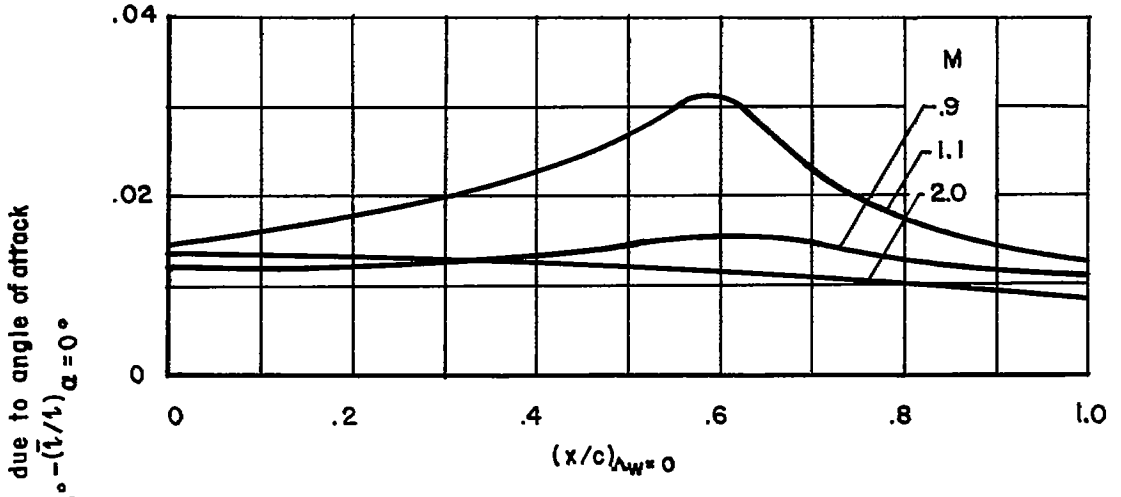

(h) Effect of wing sweep.

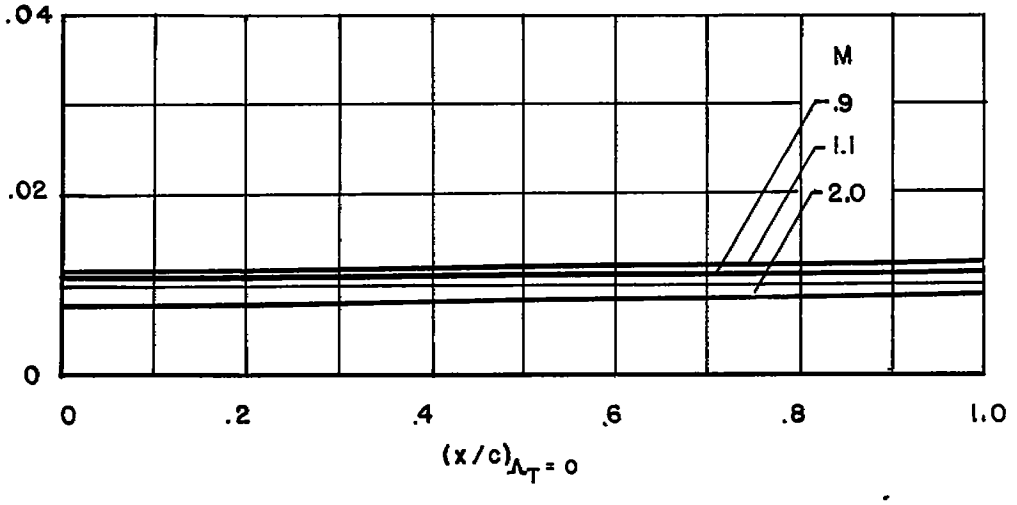

(i) Effect of tail sweep.

Figure 4.- Concluded.

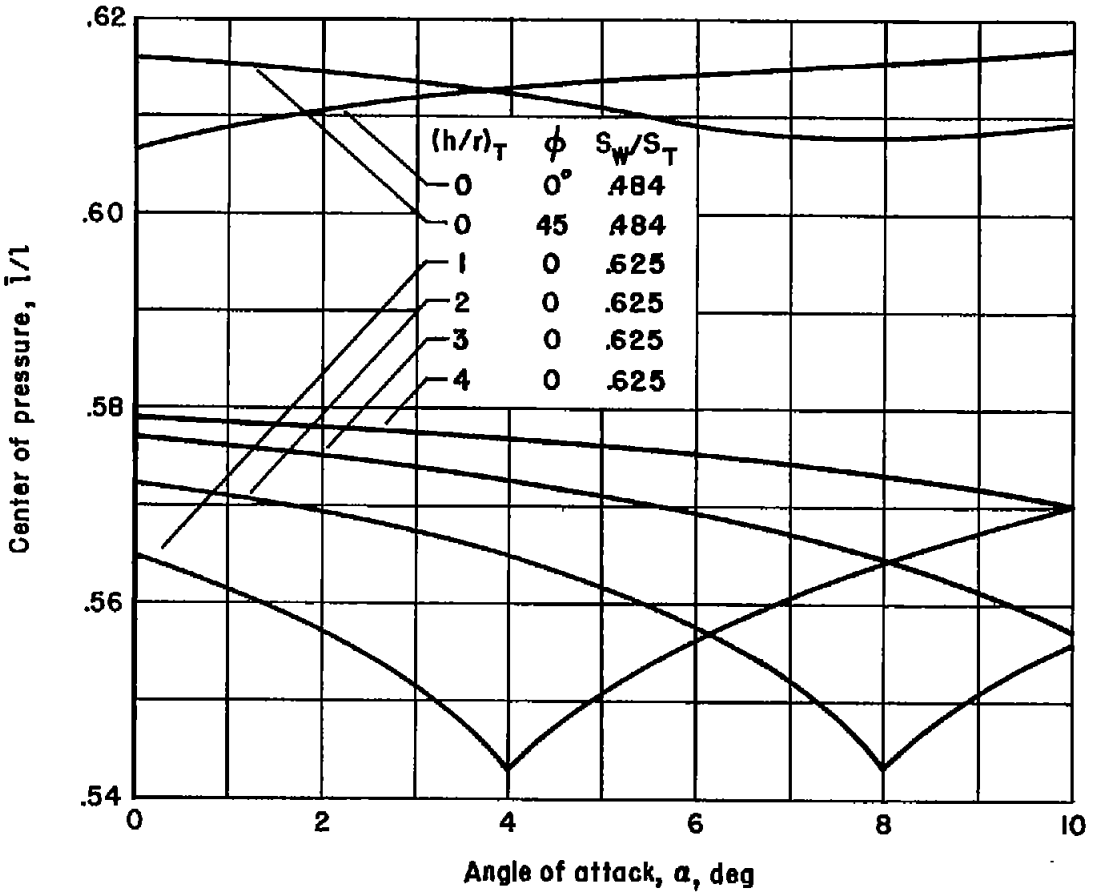

Figure 5.- Effects of tail height and rotation on the variation of center of pressure with angle of attack, M = 2.0.

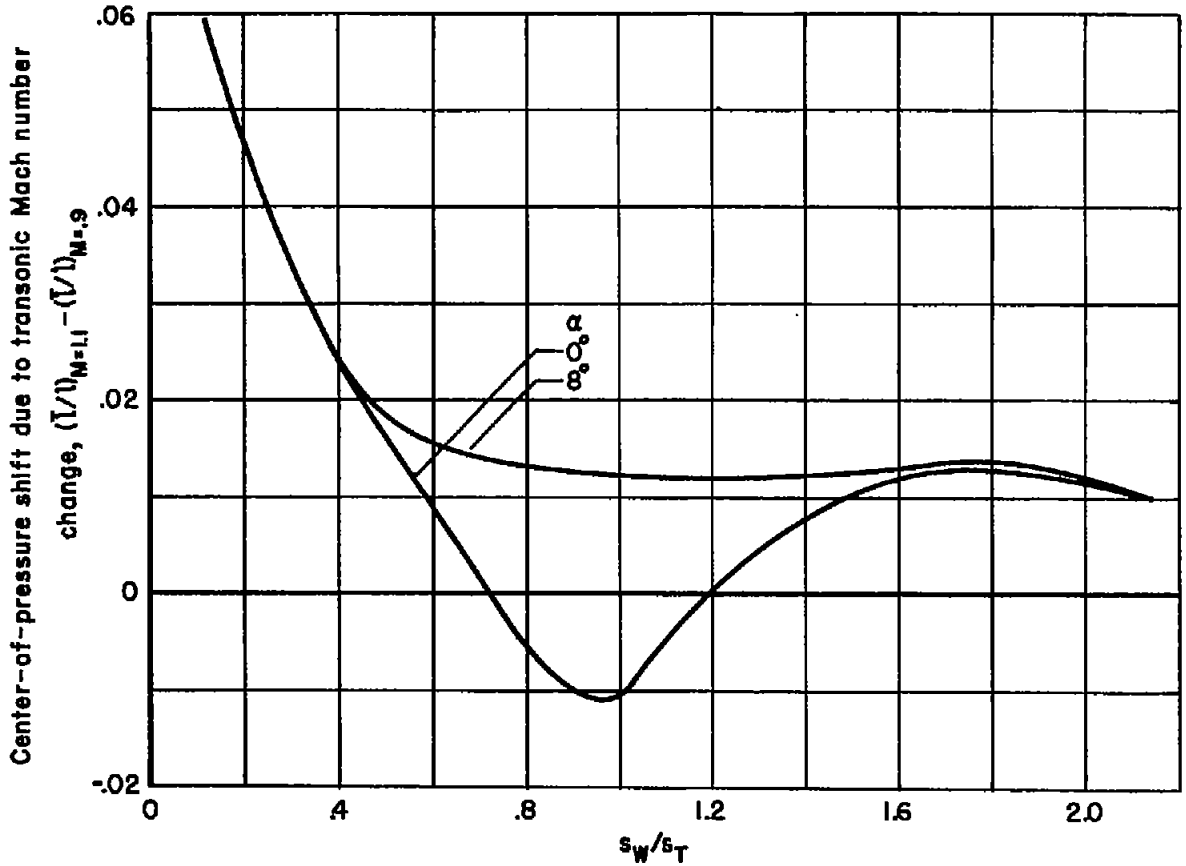

(a) Effect of wing-semispan to tail-semispan ratio.

Figure 6.- Effects of geometric parameters on the center-of-pressure shift due to transonic Mach number change.

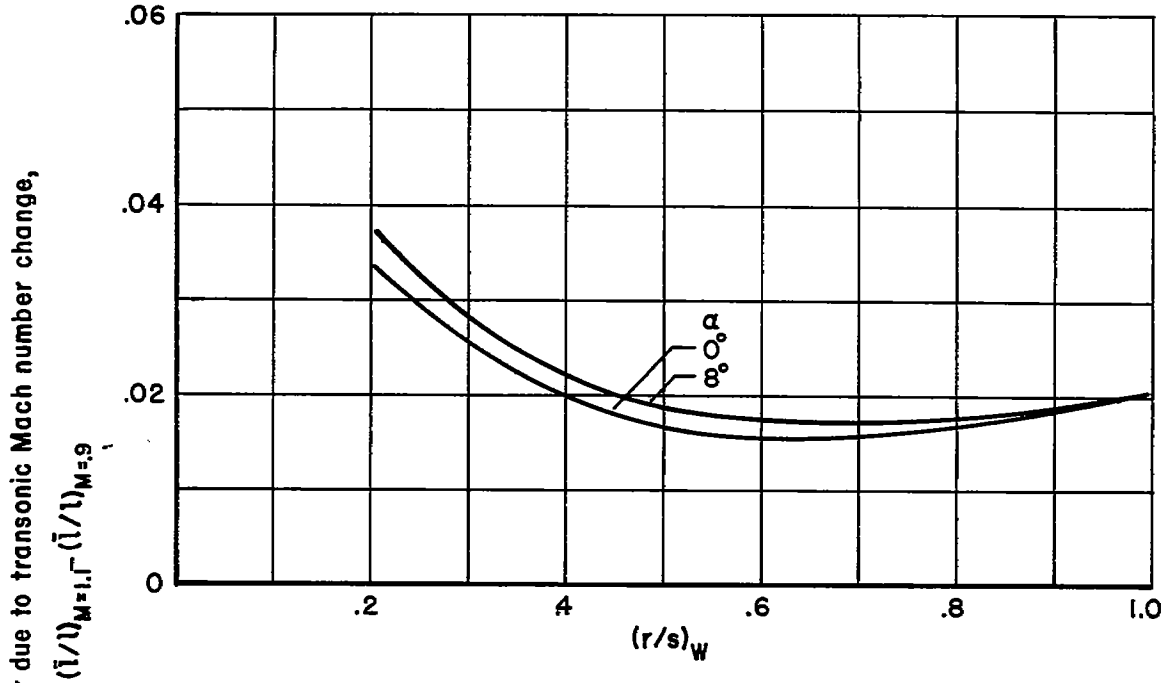

(b) Effect of body-radius to wing-semispan ratio.

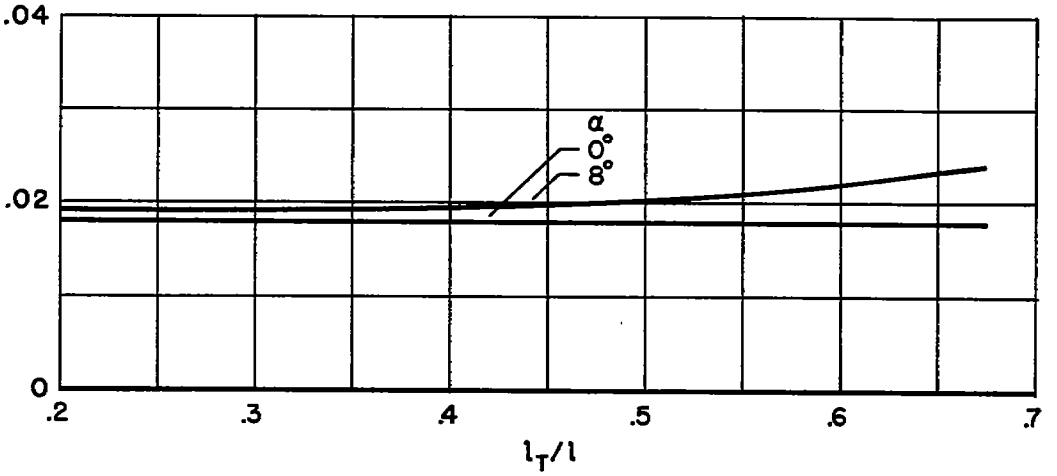

(c) Effect of tail-length to body-length ratio.

Figure 6.- Continued.

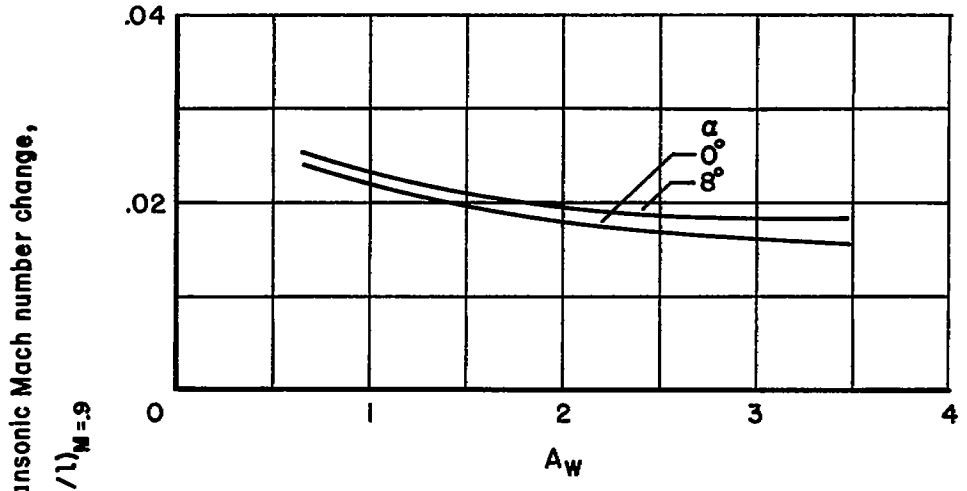

(d) Effect of wing aspect ratio.

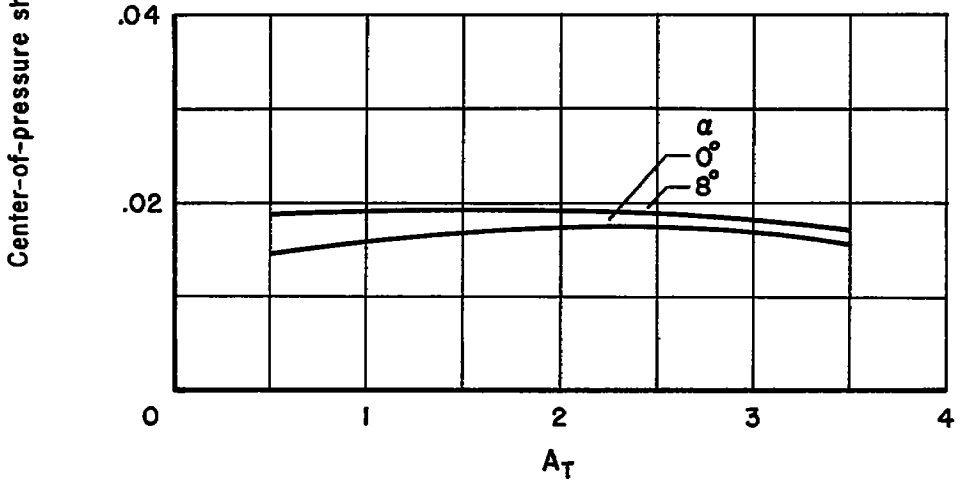

(e) Effect of tail aspect ratio.

Figure 6.- Continued.

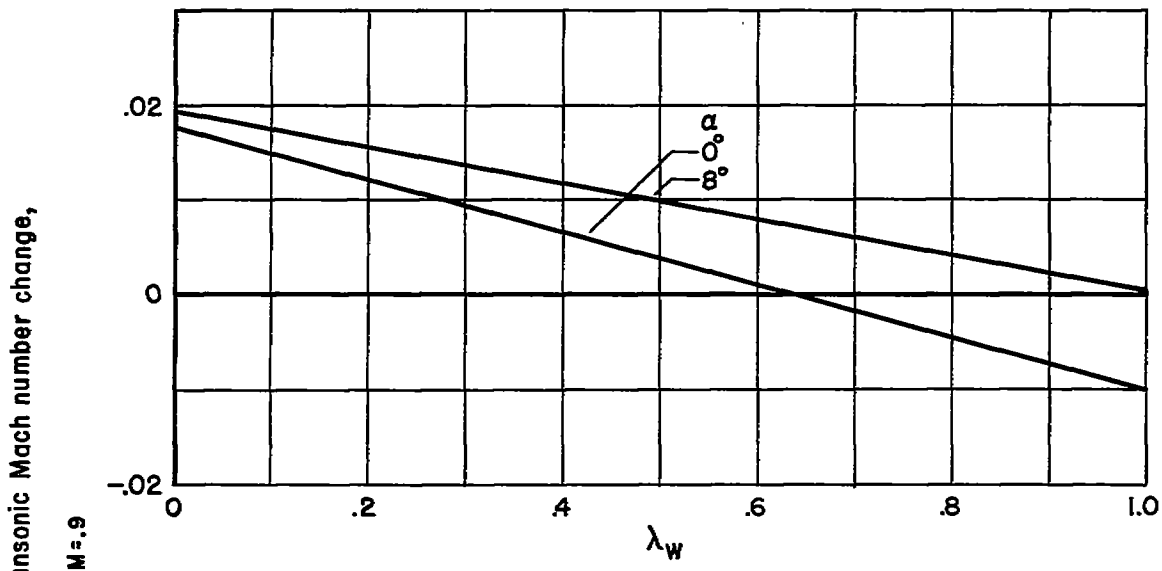

(f) Effect of wing taper ratio.

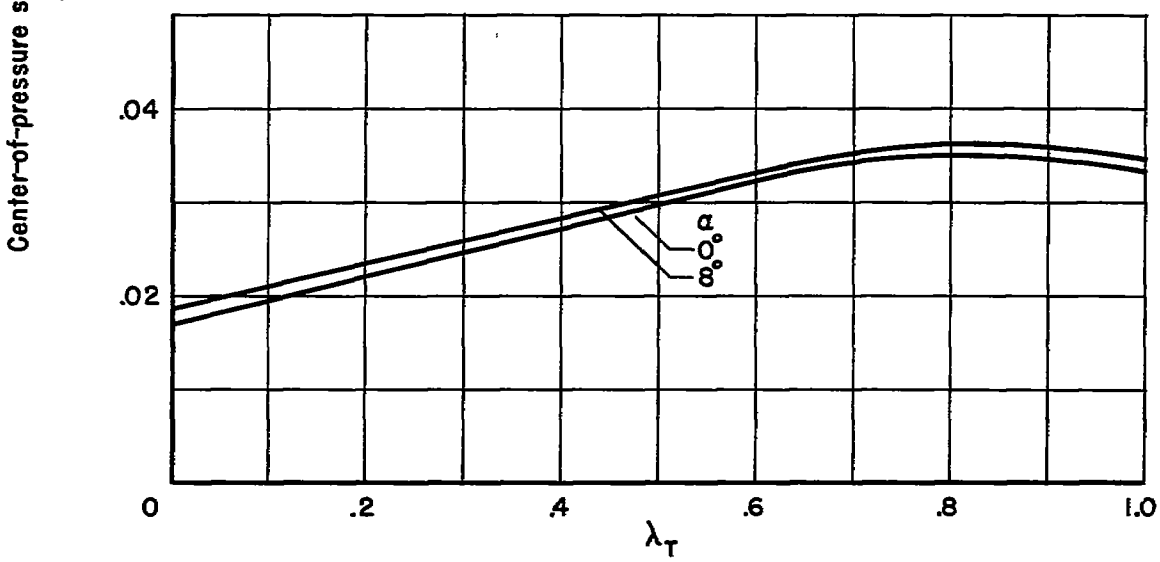

(g) Effect of tail taper ratio.

Figure 6.- Continued.

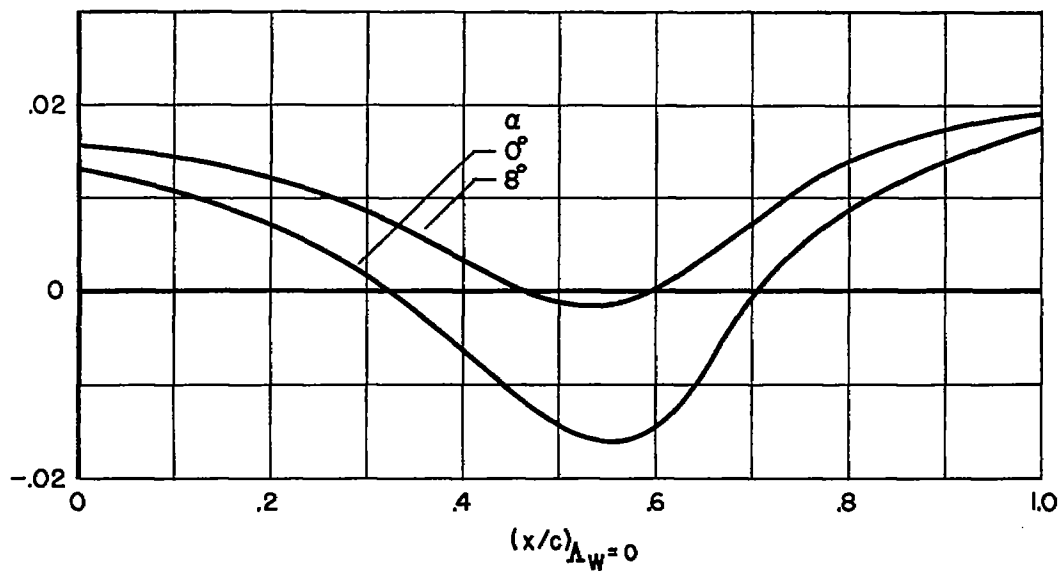

(h) Effect of wing sweep.

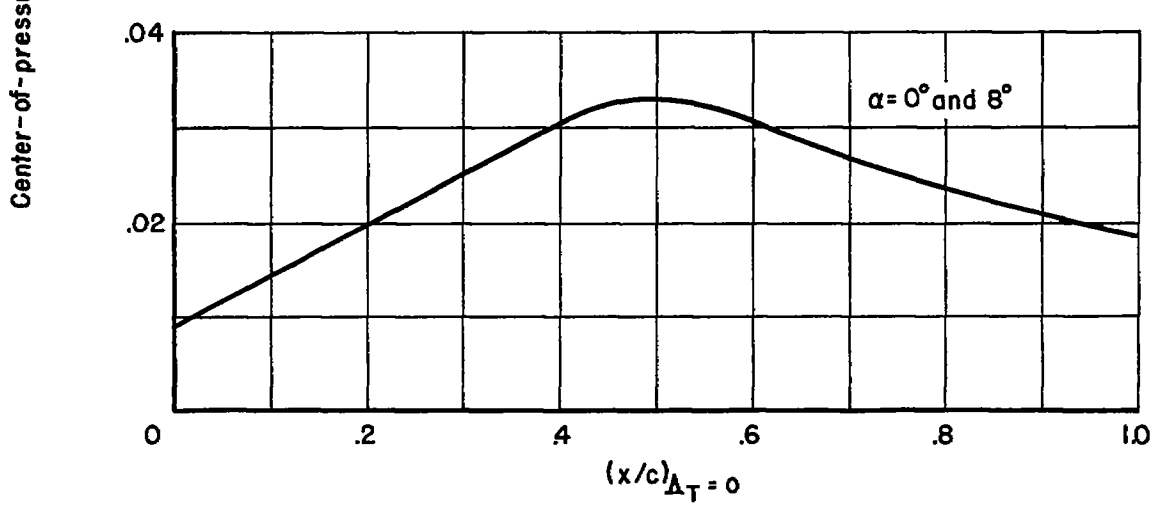

(i) Effect of tail sweep.

Figure 6.- Concluded.

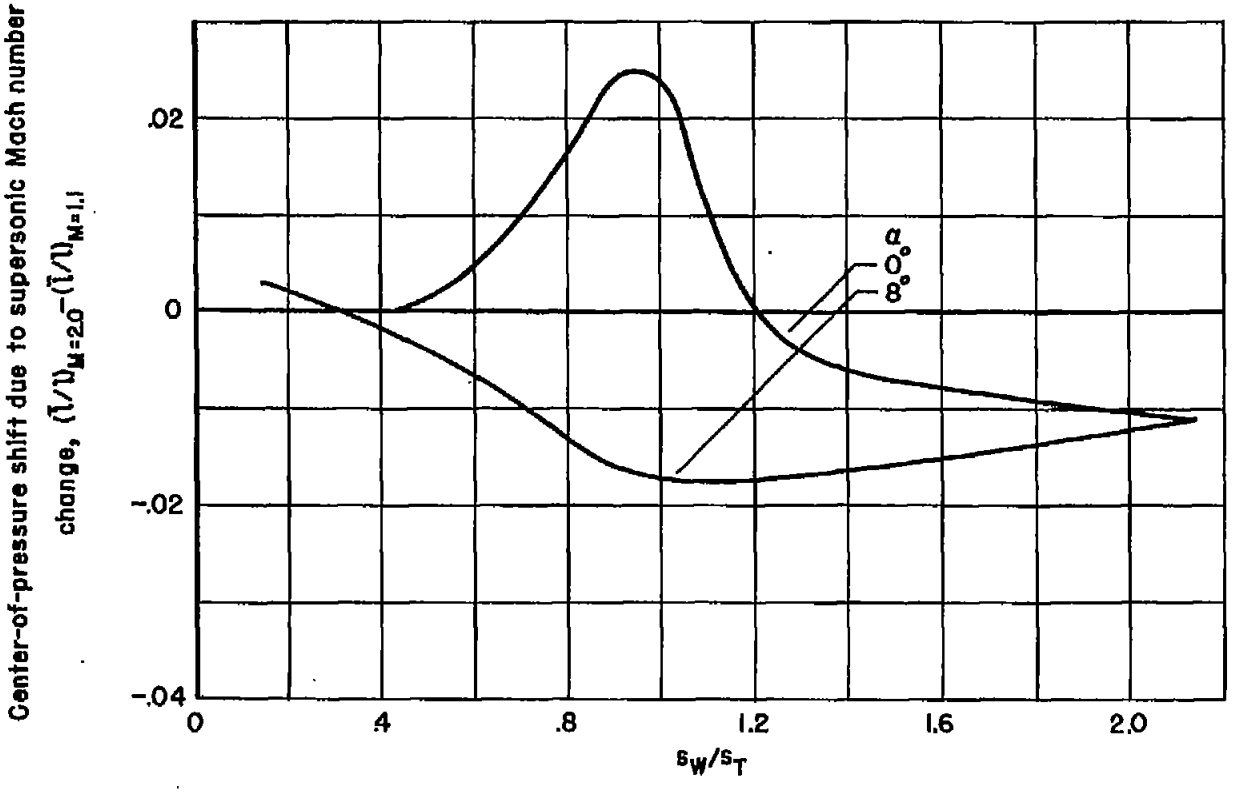

(a) Effect of wing-semispan to tail-semispan ratio.

Figure 7.- Effects of geometric parameters on the center-of-pressure shift due to supersonic Mach number change.

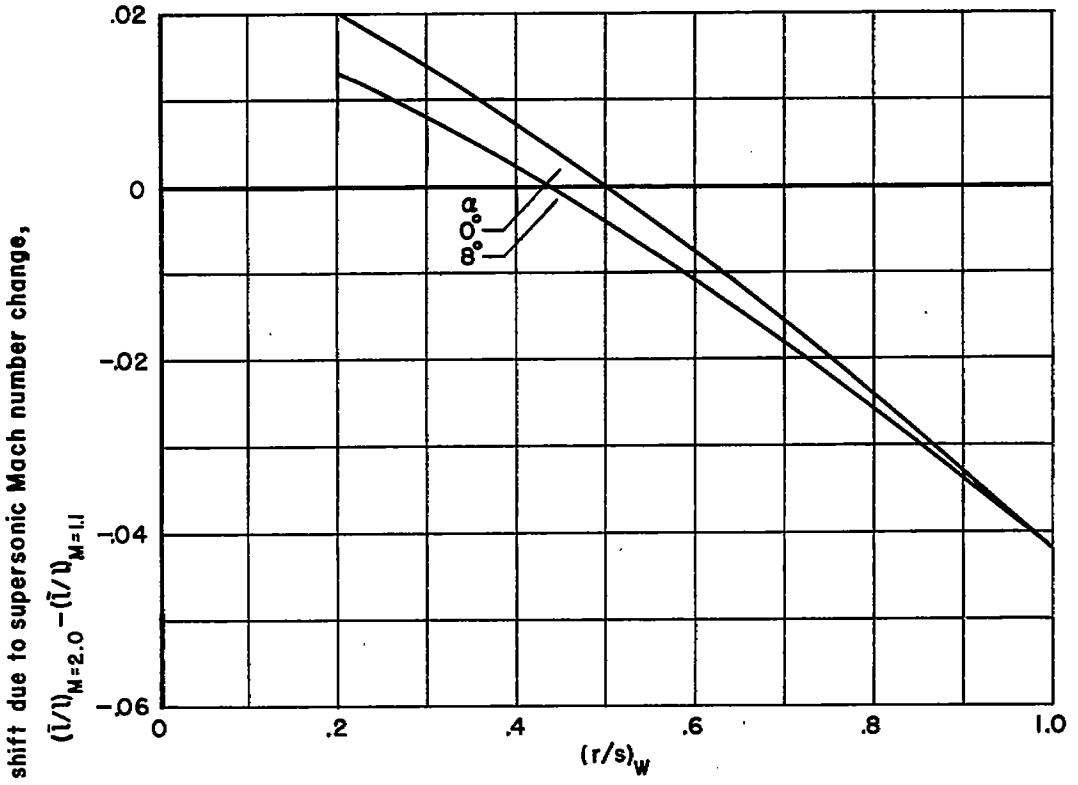

(b) Effect of body-radius to wing-semispan ratio.

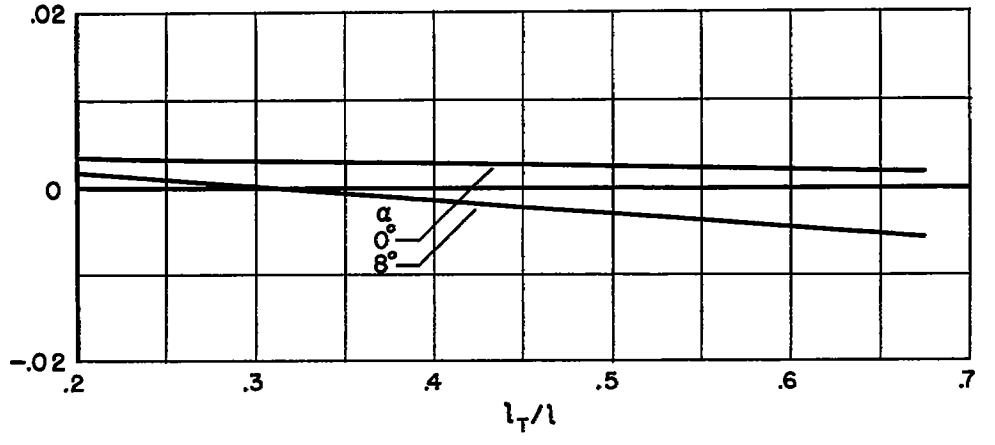

(c) Effect of tail-length to body-length ratio.

Figure 7.- Continued.

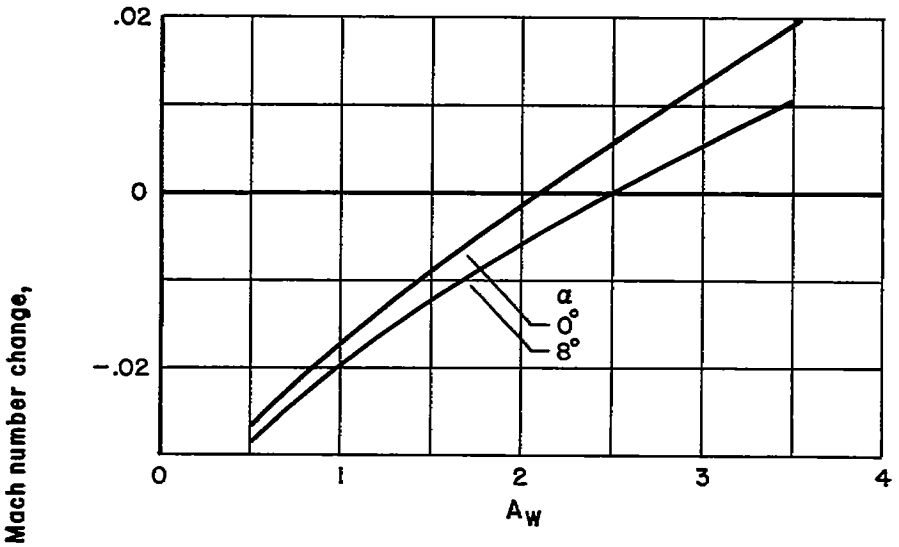

(d) Effect of wing aspect ratio.

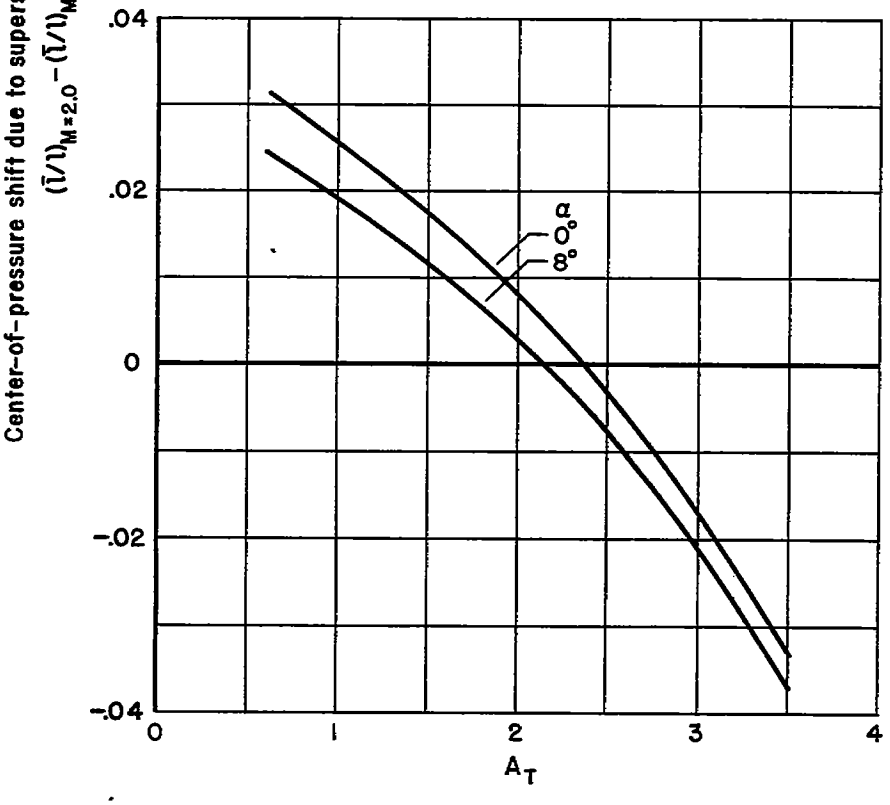

(e) Effect of tail aspect ratio.

Figure 7.- Continued.

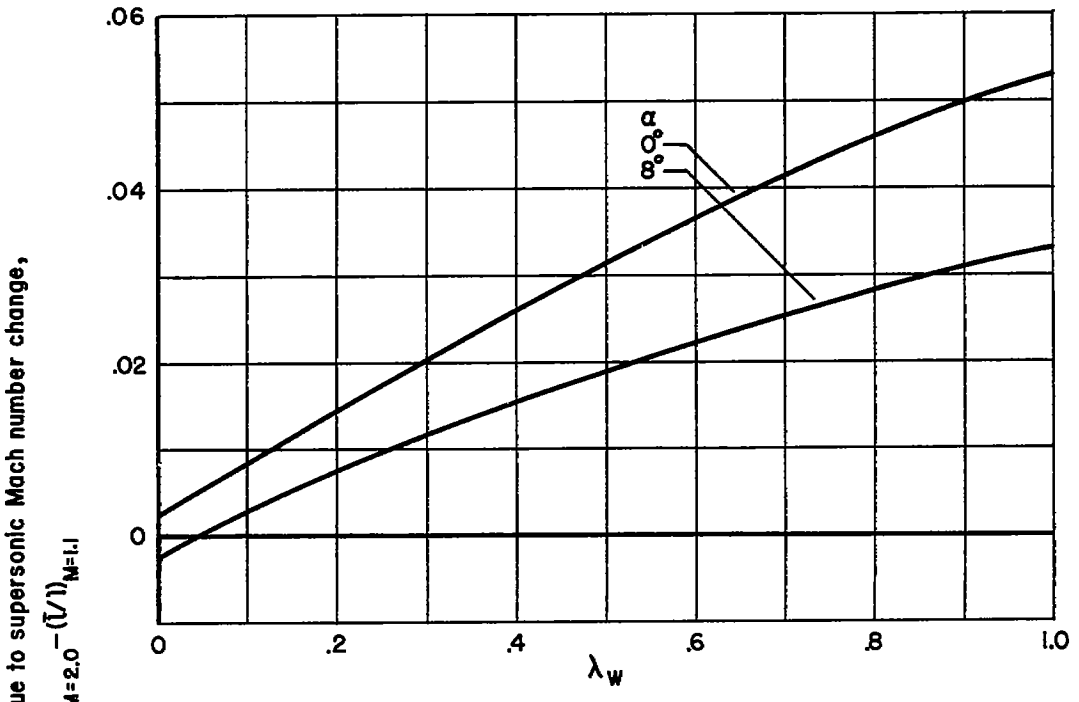

(f) Effect of wing taper ratio.

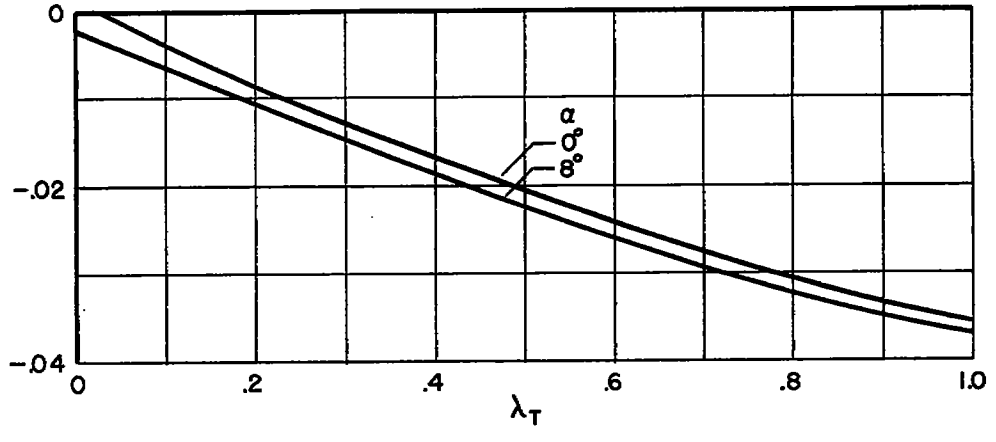

(g) Effect of tail taper ratio.

Figure 7.- Continued.

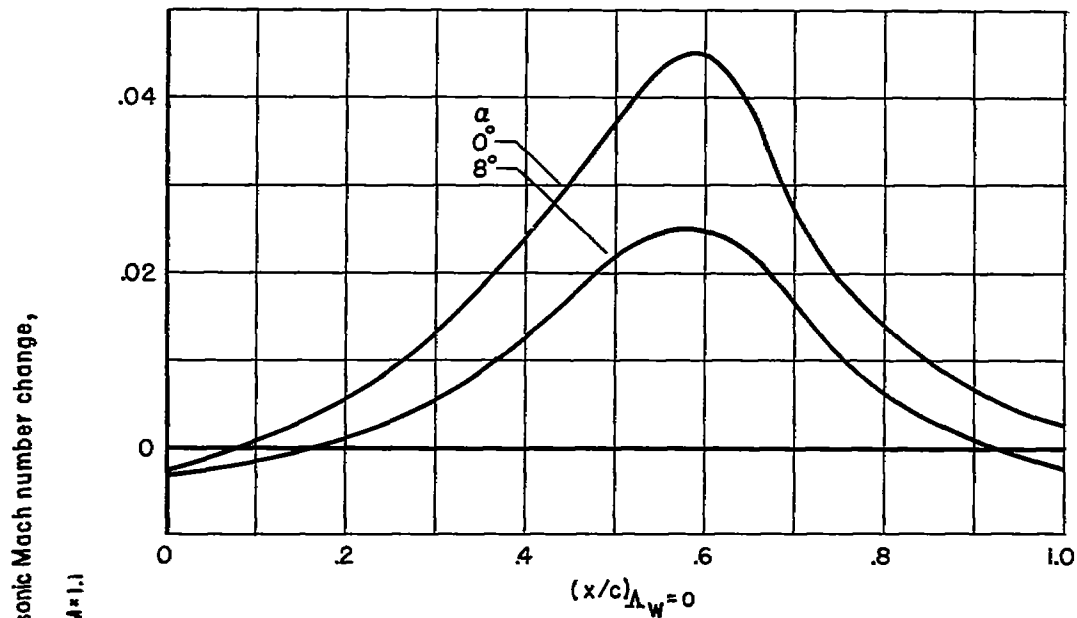

(h) Effect of wing sweep.

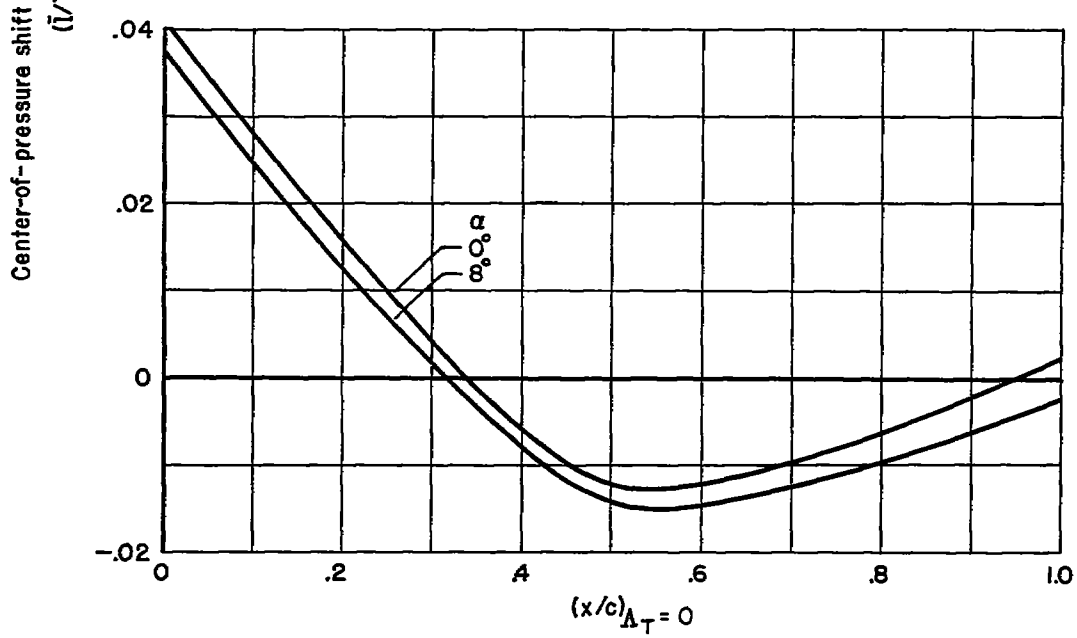

(i) Effect of tail sweep.

Figure 7.- Concluded.